Growth-dependent activation of protein kinases links cell cycle progression to cell growth

Akshi Jasani, Tiffany Huynh, and Douglas R. Kellogg

Department of Molecular, Cell, and Developmental Biology, University of California, Santa Cruz, Santa Cruz, CA 95064, USA

Abstract

In all cells, progression through the cell cycle occurs only when sufficient growth has occurred. This fundamental linkage shows that cells can measure growth, but the underlying mechanisms are poorly understood. Here, we investigate how budding yeast cells measure growth. Cells that lack the related kinases Gin4 and Hsl1 show excessive bud growth during a prolonged cell cycle delay, which suggests that they fail to detect bud growth. Moreover, Gin4 and Hsl1 undergo hyperphosphorylation that is proportional to bud growth and dependent upon binding to anionic phospholipids that are delivered to the growing bud. Gin4 and Hsl1 have previously been shown to relay signals that control both cell growth and cell cycle progression. Together, the data suggest that addition of phospholipids to the plasma membrane generates a gradually increasing signal that triggers cell cycle progression when sufficient growth has occurred. The data further suggest that control of cell size and cell growth are mechanistically linked.

Introduction

Key cell cycle transitions occur only when sufficient growth has occurred. To enforce this linkage, cells must convert growth into a proportional signal that triggers cell cycle progression when it reaches a threshold. The molecular mechanisms by which cells generate proportional signals that are used to measure and limit growth have remained deeply mysterious.

In budding yeast, growth occurs in three distinct intervals that are characterized by different rates and patterns of growth (Johnston *et al.*, 1977; McCusker *et al.*, 2007; Goranov *et al.*, 2009; Ferrezuelo *et al.*, 2012; Leitao and Kellogg, 2017). The first interval occurs during G1 phase and is characterized by uniform growth over the cell surface. The second interval is initiated at the end of G1 phase as a new daughter cell emerges and undergoes polar growth. The third interval is initiated at entry into mitosis and is marked by a switch from polar bud growth to isotropic growth that occurs more widely over the bud surface. Bud growth continues throughout mitosis. The distinct size and shape of a yeast cell is ultimately defined by how much growth occurs during each of these intervals.

Several observations suggest that the two intervals of bud growth are tightly controlled (Leitao and Kellogg, 2017). First, a newborn daughter cell that is initiating bud emergence at the end of G1 phase typically has gained 80% of its volume during bud growth in the previous cell cycle. Little growth occurs during G1 phase. Furthermore, most bud growth occurs during mitosis, and the rate of growth in mitosis is approximately 3-fold faster than the rate of growth during the other intervals. Together, these observations suggest that maintenance of a specific cell size requires tight control over the duration and extent of bud growth.

Additional evidence that bud growth is tightly controlled comes from analysis of the effects of nutrients on cell growth and size. Shifting cells from rich to poor nutrients causes a reduced growth rate, as well as a large reduction in cell size (Johnston *et al.*, 1977; 1979). This proportional relationship between growth rate and cell size appears to hold across all orders of life. In budding yeast, a shift to poor nutrients has little effect on cell size at completion of G1 phase (Bean *et al.*, 2006; Leitao and Kellogg, 2017). Furthermore, mutant cells that lack all known regulators of cell size in G1 phase show robust nutrient modulation of cell size (Jorgensen and Tyers, 2004a). In contrast, poor nutrients cause a large decrease in the extent of growth in both metaphase and anaphase, which causes daughter cells to complete cytokinesis at a substantially reduced cell size (Hartwell and Unger, 1977; Leitao and Kellogg, 2017). Furthermore, the duration of the metaphase and anaphase growth intervals is increased in poor nutrients, which suggests that cells compensate for slow bud growth by increasing the duration of growth (Leitao and Kellogg, 2017). These observations point to the existence of mechanisms that measure and modulate both the duration and extent of bud growth during mitosis.

A model in which the extent of bud growth is tightly controlled requires a molecular mechanism for measuring growth. In previous work, we found evidence that polar growth of the bud before mitosis is measured via growth-dependent hyperphosphorylation and activation of the protein kinase Pkc1 (Anastasia *et al.*, 2012). The data suggest a model in which the vesicles that drive polar growth of the plasma membrane carry signaling molecules that drive activation of Pkc1 at the site of membrane growth, thereby generating a signal that is proportional to the extent of growth. Here, we searched for proteins that could play a similar role in measuring growth during mitosis. A candidate search identified 3 related kinases: Gin4, Hsl1 and Kcc4. We refer to these as Gin4-related kinases. Similar kinases are found in all eukaryotes. Observations reaching back over 30 years have suggested that Gin4-related kinases play critical roles in control of cell growth and size (Young and Fantes, 1987; Altman and Kellogg, 1997; Ma et al., 1996a; Okuzaki et al.,

1997; Barral et al., 1999). For example, loss of Gin4-related kinases in budding yeast causes a prolonged metaphase delay (Altman and Kellogg, 1997; Ma et al., 1996a; Barral et al., 1999). Growth continues during the delay, resulting in aberrant growth of very large cells (Altman and Kellogg, 1997; Okuzaki *et al.*, 1997; Barral *et al.*, 1999). Thus, cells that lack Gin4-related kinases behave as though they cannot detect that growth has occurred during mitosis. Gin4-related kinases are localized to the bud neck throughout bud growth, so they are well-positioned to control growth (Barral et al., 1999; Longtine et al., 2000; Okuzaki et al., 1997). Moreover, we previously found that Gin4 undergoes gradual hyperphosphorylation and activation during bud growth that reaches a peak in late mitosis as growth ends (Altman and Kellogg, 1997). This discovery suggests that hyperphosphorylation and activation of Gin4 could provide a proportional readout of the extent of bud growth. To test this hypothesis, we investigated the relationship between Gin4-related kinases and bud growth.

Results

Hyperphosphorylation of Gin4 and Hsl1 is proportional to the extent of bud growth

Gin4 and Hsl1 are the most important Gin4-related kinases in budding yeast. Loss of either kinase alone causes defects in control of bud growth, whereas loss of both causes severe defects (Barral *et al.*, 1999; Longtine *et al.*, 2000). Loss of Kcc4 has little effect. We therefore focused on Gin4 and Hsl1. In previous work we discovered that Gin4 undergoes gradual hyperphosphorylation and activation during bud growth, which suggested that it could be responding to growth-dependent signals (Altman and Kellogg, 1997). To investigate further, we first tested whether hyperphosphorylation of Gin4 and Hsl1 is proportional to bud growth. To do this, we took advantage of the fact that the duration of bud growth in mitosis is increased when cells are growing slowly on a poor carbon source, even as the extent of growth is reduced (Leitao et al., 2017). Thus, cells growing in poor carbon spend more time growing in mitosis, but complete mitosis at a reduced daughter bud size. Therefore, if hyperphosphorylation of Gin4 and Hsl1 is proportional to bud growth, the time required to reach full hyperphosphorylation should be increased in cells growing in poor carbon.

Wildtype cells growing in rich carbon (2% glucose) or poor carbon (2% glycerol, 2% ethanol) were released from a G1 arrest and phosphorylation of Gin4 and Hsl1 was assayed by western blot to detect phosphorylation events that cause electrophoretic mobility shifts. The same samples were also probed for the mitotic cyclin Clb2 as a marker for mitotic duration. Cells growing in poor carbon showed delayed mitotic entry and a prolonged mitosis compared to cells growing in rich carbon, as previously described (**Fig. 1, A and B**) (Leitao and Kellogg, 2017). Previous work has shown that Gin4 is present throughout the cell cycle, while Hsl1 is synthesized anew before mitosis and destroyed at the end of mitosis (Altman and Kellogg, 1997; Barral *et al.*, 1999). In both carbon sources, hyperphosphorylation of Gin4 and Hsl1 increased gradually during mitosis, with peak phosphorylation occurring near peak Clb2 levels. In addition, the interval during which hyperphosphorylation occurred was prolonged in poor carbon, consistent with the hypothesis that hyperphosphorylation of Gin4 and Hsl1 provides a readout of the extent of bud growth.

We also noticed that the maximal extent of phosphorylation of Gin4 and Hsl1 was reduced in poor carbon (**Fig. 1, A, B and C**). Thus, cells in poor carbon progress through mitosis with less hyperphosphorylation of Gin4 and Hsl1 than cells in rich carbon, which suggests that the maximal extent of hyperphosphorylation of Gin4 and Hsl1 reached during mitosis is proportional to the growth rate set by the carbon source. One interpretation of this observation is that the extent of hyperphosphorylation of Gin4 and Hsl1 required for mitotic exit is reduced in poor carbon, which allows cells to complete mitosis at a smaller bud size.

Hyperphosphorylation of Gin4 is dependent upon bud growth

We next tested whether hyperphosphorylation of Gin4 is dependent upon bud growth. To do this, we used a temperature-sensitive allele of *SEC6* (*sec6-4*) to block bud growth. Sec6 is a component of the exocyst complex, which is required at the plasma membrane for docking and fusion of vesicles that drive bud growth. In previous work, we showed that inactivation of Sec6 blocks bud growth and triggers an arrest in early mitosis (Anastasia *et al.*, 2012). The arrest is enforced by Swe1, the budding yeast homolog of the Wee1 kinase that phosphorylates and inhibits mitotic Cdk1. Thus, *sec6-4 swe1*Δ cells fail to undergo bud growth yet enter mitosis and complete chromosome segregation before arresting in late mitosis. We therefore analyzed Gin4

phosphorylation in *sec6-4 swe1*Δ cells, which allowed us to distinguish whether effects of *sec6-4* were a consequence of a failure to undergo bud growth, or a failure to enter mitosis. As controls, we also analyzed Gin4 hyperphosphorylation in wild type and *swe1*Δ cells.

Cells were released from a G1 arrest and shifted to the restrictive temperature for the *sec6-4* allele before bud emergence. Gin4 phosphorylation was assayed by western blot (**Fig. 2 A**). The same samples were probed for Clb2 as a marker for mitotic progression (**Fig. 2 B**). The *sec6-4 swe1*Δ cells entered mitosis but arrested in late mitosis with high levels of mitotic cyclin, as previously reported (Anastasia *et al.*, 2012). Hyperphosphorylation of Gin4 failed to occur in the *sec6-4 swe1*Δ cells (**Fig. 2, A and C**). Direct comparison of the extent of Gin4 hyperphosphorylation in mitosis showed a complete loss of Gin4 phosphorylation (**Fig. 2 C**). Thus, hyperphosphorylation of Gin4 is dependent upon membrane trafficking events that drive bud growth.

Gin4 and Hsl1 are required for normal control of bud growth during mitosis

We next investigated whether Gin4 and Hsl1 are required for normal control of daughter cell growth in mitosis. Previous studies found that loss of Gin4 and/or Hsl1 causes prolonged bud growth during a mitotic delay, consistent with the hypothesis that Gin4 and Hsl1 play a role in growth sensing (Ma *et al.*, 1996b; Altman and Kellogg, 1997; Barral *et al.*, 1999). However, previous studies were carried out with gene deletions, which made it difficult to discern whether loss of growth control was an immediate and direct consequence of loss of Gin4 or Hsl1. We therefore created auxin-inducible degron (AID) versions of Gin4 and Hsl1, which allowed us to analyze the immediate effects of conditional inactivation (Nishimura *et al.*, 2009). A strain carrying AID-tagged versions of both *GIN4* and *HSL1* had no size defects in the absence of auxin (**Fig. S1 A**). Addition of auxin before mitosis in synchronized cells caused a large reduction in levels of Gin4-AID protein within 30 minutes (**Fig. S1 B**), as well as a delay in mitotic progression (**Fig. S1 C**).

Gin4 and Hsl1 control Swe1, which undergoes complex regulation in mitosis (Harvey et al., 2011; 2005). In early mitosis, Cdk1 phosphorylates Swe1 on Cdk1 consensus sites, which activates Swe1 to bind and inhibit Cdk1. This form of Swe1, which we refer to as partially hyperphosphorylated Swe1, works in a systems-level mechanism that maintains a low level of Cdk1 during metaphase. Further phosphorylation events drive full hyperphosphorylation of Swe1, leading to release of Cdk1 and inactivation of Swe1. Swe1 is proteolytically destroyed at the end of mitosis; however, mutants that block Swe1 destruction have no effect on mitotic progression, so the function of Swe1 destruction remains unknown (Thornton and Toczyski, 2003; Raspelli *et al.*, 2011).

A previous study suggested that *hsl1*Δ causes defects in phosphorylation of Swe1 (Shulewitz *et al.*, 1999). Here, we found that conditional inactivation of gin4-AID and hsl1-AID before mitosis in synchronized cells caused a failure in full hyperphosphorylation of Swe1 (**Fig. 3 A**). Similarly, addition of auxin to asynchronous *gin4-AID hsl1-AID* cells caused loss of fully hyperphosphorylated Swe1 within 30 minutes (**Fig. S1 D**). These data provide further evidence that Gin4 and Hsl1 control mitotic progression via regulation of Swe1.

We next tested how conditional inactivation of Gin4 and Hsl1 influences bud growth and mitotic progression in single cells. We included a fluorescently tagged spindle pole protein to monitor the duration of metaphase and anaphase (Leitao and Kellogg, 2017). The spindle poles in wild type and *gin4-AID hsl1-AID* cells were marked with different fluorescent tags, which allowed simultaneous imaging of both strains under identical conditions.

We analyzed the effects of *gin4-AID* or *hsl1-AID* alone, as well as the effects of *gin4-AID hsl1-AID*. Cells were released from a G1 arrest and auxin was added before initiation of bud emergence, which ensured that Gin4 and Hsl1 were depleted by the time of mitotic entry. Bud size and mitotic spindle dynamics were then analyzed at 3-minute intervals to determine how loss of Gin4 and Hsl1 influenced bud growth and the duration of mitosis. Examples of wild type and *gin4-AID hsl1-AID* cells are shown in **Fig. 3 B and Video 1**. Both cells undergo bud emergence at nearly the same time, but the wild type cell completes bud growth and exits mitosis while the *gin4-AID hsl1-AID* cell remains delayed in metaphase as the bud continues to grow. The *gin4-AID hsl1-AID* cell eventually completes mitosis, but at a substantially larger bud size than the wild type control cell. The daughter bud is more elongated in the *gin4-AID hsl1-AID* cell, which indicates a defect in control of polar growth.

Quantitative analysis of multiple cells showed that destruction of Gin4 and/or Hsl1 caused an increase in the duration of metaphase but had no effect on the duration of anaphase (**Fig. 4 A**). Destruction of Gin4 and Hsl1 also caused an increase in bud size at completion of each mitotic interval (**Fig. 4 B**). The effects of *gin4-AID* and *hsl1-AID* were not additive (**Fig. 4, A and B**), which was surprising because *hsl1*Δ and *gin4*Δ have strong additive effects on cell size and shape (**Fig. S2 A** and (Barral *et al.*, 1999)). This issue is addressed below.

In wild type cells, the bud volume reached at completion of mitosis is proportional to growth rate during mitosis (Leitao and Kellogg, 2017). *gin4-AID hsl1-AID* appeared to cause a partial loss of the proportional relationship between growth rate and cell size at completion of mitosis (**Fig. 4 C**). *gin4-AID hsl1-AID* did not cause significant effects on the growth rate of the daughter cell (**Fig. S2 B**).

Inactivation of *gin4-AID* caused polar bud growth to continue in mitosis, whereas inactivation of *hsl1-AID* did not. This effect was quantified by measuring axial ratios of daughter buds at completion of anaphase (**Fig. 4 D**).

Previous studies found that *gin4*Δ and *hsl1*Δ cause defects in cytokinesis that lead to formation of clumps of interconnected cells (Okuzaki et al., 1997; Ma et al., 1996b; Altman and Kellogg, 1997; Barral et al., 1999). Consistent with this, we observed that *gin4-AID hsl1-AID* caused a failure in cell separation in nearly all cells following the first cell cycle after addition of auxin (**Video 2**). Previous studies also found that *gin4*Δ and *hsl1*Δ cause defects in spindle positioning (Fraschini *et al.*, 2006; Grava *et al.*, 2006). We observed few defects in spindle positioning during the first cell division after addition of auxin to *gin4-AID hsl1-AID* cells. However, in the second cell division many cells showed aberrant movement of the metaphase spindle into the daughter cell before anaphase (**Video 2**).

Gin4 and Hsl1 are required for normal control of mother cell growth

In wild type cells, little growth of the mother cell occurs after bud emergence (Ferrezuelo et al., 2012; McCusker et al., 2007). In *gin4-AID hsl1-AID* cells, however, mother cell growth often continued throughout the interval of daughter cell growth. Example plots of mother and daughter cell size as a function of time for wild type and *gin4-AID hsl1-AID* cells are shown in **Fig. 5 A**. Quantitative analysis revealed that gin4-AID and hsl1-AID had additive effects upon mother cell growth so that most *gin4-AID hsl1-AID* cells underwent abnormal mother cell growth (**Fig. 5 B**).

Previous work has shown that large mother cells drive a faster rate of daughter cell growth (Schmoller *et al.*, 2015; Leitao and Kellogg, 2017). As a result, the increased size of mothers in *gin4-AID hsl1-AID* cells would be expected to drive faster growth of daughter cells in subsequent cell divisions, leading to increased defects in cell growth and size in subsequent cell divisions.

Thus, the role of Gin4 and Hsl1 in control of mother cell growth could help explain why prolonged loss of Gin4 and Hsl1 causes strong additive effects on cell growth and size. Defects in spindle positioning and cell separation could also cause increased defects in subsequent cell divisions. We found that the effects caused by *gin4-AID hsl1-AID* increased substantially with prolonged incubation in the presence of auxin, consistent with a model in which the terminal phenotype caused by *gin4*Δ *hsl1*Δ is the result of defects that accumulate over multiple cell cycles (**Fig. S3**).

Gin4-related kinases influence the duration of growth in metaphase via inhibitory phosphorylation of Cdk1

Genetic analysis has shown that Gin4 and Hsl1 are negative regulators of Swe1, and that Swe1 influences the timing of mitotic entry as well as the duration of metaphase (**Fig. 3 A**) (Ma *et al.*, 1996b; Longtine *et al.*, 2000; Harvey and Kellogg, 2003; Lianga *et al.*, 2013; (Leitao et al., 2018). We therefore tested whether Gin4 and Hsl1 influence metaphase duration via Swe1. To do this, we analyzed the effects of *swe1*Δ on bud growth and mitotic duration in *gin4-AID hsl1-AID* cells. This revealed that *swe1*Δ eliminated the prolonged metaphase delay caused by loss of Gin4 and Hsl1 (**Fig. 4 A**). Furthermore, *swe1*Δ caused daughter buds in *gin4-AID hsl1-AID* cells to complete metaphase and anaphase at sizes smaller than the wild type control cells (**Fig. 4 B**), and it eliminated the bud elongation caused by *gin4-AID* (**Fig. 4 D**). As reported previously, *swe1*Δ caused reduced growth rate, which is thought to be due to the decreased size of mother cells (**Fig. S2 B**) (Leitao *et al.*, 2018).

Several observations demonstrated that Gin4 and Hsl1 do not influence growth solely via Swe1. Previous studies found that *swe1*Δ cells have a shorter metaphase than wild type cells (Lianga *et al.*, 2013; Leitao *et al.*, 2018). Here, we found that *swe1*Δ reduced the duration of metaphase in *gin4-AID hsl1-AID* cells, but it did not make the duration of metaphase in these cells shorter than metaphase in wild type cells. In addition, *swe1*Δ did not fully rescue growth defects caused by *gin4*Δ *hsl1*Δ (**Fig. S2 A**). Finally, *swe1*Δ did not eliminate inappropriate growth of mother cells in *gin4-AID hsl1-AID* cells (**Fig. 5 B**). Together, these observations demonstrate that Gin4 and Hsl1 control bud growth during mitosis through Swe1-dependent and Swe1-independent mechanisms.

Proportional phosphorylation of Gin4 during bud growth requires binding to anionic phospholipids

We next searched for a mechanism that could explain how hyperphosphorylation of Gin4 and Hsl1 is linked to bud growth. Both Gin4 and Hsl1 have well-defined C-terminal kinase associated 1 (KA1) domains, which bind phosphatidylserine and other anionic phospholipids (Moravcevic *et al.*, 2010). In vivo analysis suggests that phosphatidylserine is the most important effector for KA1 domains (Moravcevic *et al.*, 2010). Phosphatidylserine is a low abundance phospholipid that is preferentially localized to the growing bud (Fairn et al., 2011; Ejsing et al., 2009; Klose et al., 2012). Furthermore, binding of phosphatidylserine to kinases that contain KA1 domains can promote an open and active conformation of the kinase that could potentially drive autophosphorylation or phosphorylation by another kinase (Wu *et al.*, 2015; Emptage *et al.*, 2017; 2018). Together, these observations led us to hypothesize that phosphatidylserine delivered to the plasma membrane during bud growth drives hyperphosphorylation of Gin4-related kinases, thereby generating a signal that is proportional to the extent of growth.

To test the hypothesis, we focused on Gin4. A version of Gin4 that lacks the KA1 domain (*gin4-*Δ*KA1*) failed to undergo hyperphosphorylation during bud growth (**Fig. 6 A**). Analysis of

Clb2 levels in synchronized cells showed that *gin4-ΔKA1* cells exhibited normal timing of mitotic entry, but increased duration of mitosis (**Fig. 6 B**). The *gin4-ΔKA1* cells also showed increased cell size and an elongated bud phenotype similar to *gin4Δ* cells (**Fig. 6, C and D)**. *gin4-ΔKA1* in an *hsl1Δ* background caused a phenotype similar to *gin4Δ hsl1Δ* (**Fig. 6 D**). Finally, Gin4-ΔKA1-GFP failed to localize to the bud neck normally and was observed primarily in the cytoplasm (**Fig. 6 E**), although weak localization to the bud neck could be detected in a fraction of cells, indicating that determinants outside the KA1 domain contribute to Gin4 localization to the bud neck (**arrowheads, Fig. 6 E**).

The KA1 domain could carry out functions required for Gin4 hyperphosphorylation that are independent of binding to anionic phospholipids. We reasoned that if binding to anionic phospholipids is the sole function of the KA1 domain, then replacing the KA1 domain with a heterologous phosphatidylserine binding domain should restore normal Gin4 activity. To test this, we replaced the KA1 domain with the bovine LactC2 domain, which shows no structural similarity to the KA1 domain (Shao *et al.*, 2008; Moravcevic *et al.*, 2010). The LactC2 domain was sufficient to restore proportional hyperphosphorylation of Gin4 during bud growth in *gin4-ΔKA1-LactC2* cells (**Fig. 6 A**). In addition, *gin4-ΔKA1-LactC2* cells showed normal mitotic timing, as well as normal cell size (**Fig. 6, B, C and D)**. Finally, the LactC2 domain restored normal bud neck localization to *gin4-ΔKA1* (**Fig. 6 E**). A previous study showed that deletion of the KA1 domain of Hsl1 causes reduced localization of Hsl1 to the bud neck, which can be rescued by addition of the LactC2 domain (Finnigan *et al.*, 2016).

Mutation of three amino acids in the LactC2 domain required for efficient binding to phosphatidylserine (*gin4-ΔKA1-LactC2^{AAA}*) (Yeung *et al.*, 2008) caused a failure in proportional phosphorylation of Gin4 (**Fig. 6 A**), as well as a phenotype similar to *gin4Δ* and *gin4-ΔKA1* (**Fig. 6, B, C and D**). The *LactC2^{AAA}* domain partially restored Gin4 localization to the bud neck, however, the amount of *gin4-ΔKA1-LactC2^{AAA}-GFP* at the bud neck was reduced relative to *GIN4-GFP* and *gin4-ΔKA1-LactC2-GFP* (**Figs. 6 E and S4**).

Discussion

Growth-dependent signals are required for control of cell growth and size

Gin4 undergoes gradual hyperphosphorylation that is dependent upon and proportional to bud growth. In addition, the kinase activity of Gin4 is dependent upon and proportional to Gin4 hyperphosphorylation (Altman and Kellogg, 1997; Mortensen *et al.*, 2002). Together, these observations suggest that the events of bud growth generate growth-dependent signals that are proportional to the extent of growth. We hypothesize that these growth-dependent signals are used to measure the extent of bud growth. They could also be used to ensure that growth rate scales with cell size. For example, the Gin4-related kinases are required for normal levels of signaling in the TORC2 network, which plays a central role in control of cell growth (Alcaide-Gavilan *et al.*, 2018). Thus, growth-dependent activation of Gin4-related kinases could drive a gradual increase in TORC2 activity that drives a gradual increase in growth rate as cells increase in size.

Growth in poor nutrient conditions that reduce both growth rate and cell size caused a reduction in the maximal extent of hyperphosphorylation of Gin4 and Hsl1. Poor nutrient conditions also cause a reduction in TORC2 signaling (Lucena *et al.*, 2018). These observations are consistent with the idea that signals from the Gin4-related kinases play a role in setting the level of TORC2 signaling to achieve an appropriate growth rate. They also suggest that the reduction in cell size at completion of metaphase in poor nutrients (Leitao and Kellogg, 2017) could be driven by a mechanism that reduces the threshold activity of the Gin4-related kinases required for mitotic progression.

Growth-dependent hyperphosphorylation of Gin4 requires binding to anionic phospholipids

Growth-dependent hyperphosphorylation of Gin4 and normal control of cell growth are both dependent upon the KA1 domain, which binds anionic phospholipids (Moravcevic *et al.*, 2010). The KA1 domain can be functionally replaced by a heterologous LactC2 domain that binds phosphatidylserine, and mutations in the LactC2 domain that reduce binding to phosphatidylserine also block growth-dependent phosphorylation of Gin4 and cause a failure in control of cell growth. Hyperphosphorylation of both Gin4 and Hsl1 is dependent upon their kinase activity, which suggests that growth-dependent phosphorylation is due to autophosphorylation (Altman and Kellogg, 1997; Barral *et al.*, 1999). Moreover, previous studies have suggested that binding of anionic phospholipids to KA1 domains can drive formation of an open, active conformation (Wu *et al.*, 2015; Emptage *et al.*, 2017; 2018). Together, these observations suggest that anionic phospholipids delivered to the growing bud could generate a growth-dependent signal by binding and activating Gin4-related kinases. In this model, the Gin4-related kinases would be direct sensors of a critical event that drives cell growth (i.e. delivery of anionic phospholipids to the plasma membrane).

Although there is compelling evidence that binding of phosphatidylserine is the key event that drives proportional phosphorylation of Gin4-related kinases, alternative models remain possible. For example, binding to anionic phospholipids could help bring Gin4-related kinases to the bud neck where they receive growth-dependent signals from other kinases. However, several observations argue against this kind of model. First, extensive data suggest that proportional phosphorylation of Gin4-related kinases is due to autophosphorylation (Altman and Kellogg, 1997; Barral et al., 1999; Mortensen et al., 2002). Second, gin4-ΔKA1-LactC2^{AAA} localizes to the bud

neck but fails to undergo phosphorylation, which suggests that localization to the bud neck is not sufficient for hyperphosphorylation of Gin4. Further testing of models will require biochemical reconstitution and in vivo analysis to learn more about the signals that drive growth-dependent phosphorylation of Gin4-related kinases.

The KA1 domain binds preferentially to phosphatidylserine but can also bind other anionic phospholipids, such as phosphatidylinositol (Moravcevic *et al.*, 2010; Wu *et al.*, 2015). In contrast, the LactC2 domain appears to bind only to phosphatidylserine (Shao *et al.*, 2008). The fact that the KA1 domain can be functionally replaced by the LactC2 domain therefore suggests that binding to phosphatidylserine is sufficient to generate a growth-dependent signal. Phosphatidylserine is a low abundance lipid that is preferentially localized to the growing bud (Moravcevic *et al.*, 2010; Fairn *et al.*, 2011). Phosphatidylserine is also preferentially localized to sites of membrane growth in fission yeast (Haupt and Minc, 2017).

Cells that completely lack phosphatidylserine can be made by deleting the CHO1 gene, which encodes the enzyme that catalyzes the last step in synthesis of phosphatidylserine. However, interpretation of the phenotype caused by loss of phosphatidylserine is complicated by several factors. First, loss of phosphatidylserine causes increased synthesis of phosphatidylinositol, an anionic phospholipid that could compensate for some functions of phosphatidylserine, including binding to KA1 domains (Matsuo et al., 2007; Hikiji et al., 1988). In addition, phosphatidylserine is a precursor in one of the major pathways used to synthesize phosphatidylethanolamine (Klug and Daum, 2014). In both budding yeast and fission yeast, cells that lack phosphatidylserine are barely viable (Matsuo et al., 2007; Hikiji et al., 1988). In fission yeast, the slow growth caused by loss of phosphatidylserine can be rescued by inclusion of ethanolamine in the growth media (Matsuo *et al.*, 2007). Cells grown under these conditions are abnormally large, consistent with the idea that growth-dependent signals generated by phosphatidylserine are used to determine when sufficient growth has occurred (Haupt and Minc, 2017).

Gin4-related kinases control the duration of growth in metaphase partly via Cdk1 inhibitory phosphorylation

Early work suggested that Wee1 family members work solely at mitotic entry. More recent work in both vertebrates and yeast has shown that Wee1 also controls events that occur after mitotic entry (Deibler and Kirschner, 2010; Harvey *et al.*, 2011; Lianga *et al.*, 2013; Vassilopoulos *et al.*, 2014; Toledo *et al.*, 2015; Leitao and Kellogg, 2017). In budding yeast, several studies suggested that the activity of Swe1 in metaphase could be controlled by the Gin4-related kinases (Altman and Kellogg, 1997; Sreenivasan and Kellogg, 1999; Carroll et al., 1998; Sreenivasan et al., 2003; Barral et al., 1999). Here, we used conditional inactivation of Gin4 and Hsl1 to provide definitive evidence that Gin4-related kinases control the duration of metaphase via Cdk1 inhibitory phosphorylation. We also showed that loss of Gin4-related kinases causes a failure in full hyperphosphorylation of Swe1 (Sreenivasan and Kellogg, 1999). Previous studies have suggested that Gin4-related kinases directly phosphorylate Wee1 (Kanoh and Russell, 1998; Coleman et al., 1993).

Gin4-related kinases influence the location of growth

The effects of conditional inactivation of Gin4 and Hsl1 on the duration of growth in metaphase were not additive, which was surprising because *gin4*Δ and *hsl1*Δ show strong additive effects (Barral *et al.*, 1999). A potential explanation came from the discovery that loss of

Gin4-related kinases causes inappropriate mother cell growth during mitosis. In this case, the effects of inactivating Gin4 and Hsl1 were additive. Previous work found that large mother cells drive an increased growth rate in daughter cells (Schmoller *et al.*, 2015; Leitao and Kellogg, 2017). Thus, we hypothesize that the increased size of mother cells caused by loss of Gin4 and Hsl1 drives an increased rate of growth that leads to even greater aberrant growth in subsequent divisions. However, other factors likely contribute to the additive effects of *gin4*Δ and *hsl1*Δ. For example, we observed severe spindle positioning defects in the second cell division after inactivation of Gin4 and Hsl1, which could cause prolonged mitotic delays that could cause aberrant growth. Defects in growth control could also be amplified by failures in cytokinesis that create chains of conjoined cells in which the signals that control cell growth and size are no longer effectively compartmentalized.

Destruction of Gin4 caused prolonged polar growth, which suggests that Gin4 plays a role in terminating polar growth. In normal cells, the interval of polar growth is terminated by low level activation of Cdk1 at mitotic entry (Lew and Reed, 1993). Low level activation of Cdk1 appears to occur normally in *gin4*Δ cells, albeit with a delay (Altman and Kellogg, 1997). Moreover, the elongated buds and cell separation defects caused by *gin4*Δ are not fully rescued by *swe1*Δ. Together, these observations suggest that Gin4 influences polar growth at least partly via a mechanism that works downstream of or independently of Cdk1. Previous work has suggested that Gin4 binds and regulates Bnr1, a formin protein that controls the location of actin cables that deliver vesicles to sites of membrane growth (Buttery *et al.*, 2012). Bnr1 is localized to the bud neck, and loss of Bnr1 is thought to cause inappropriate polar growth because the actin cables that direct isotropic growth are lost (Pruyne *et al.*, 2004; Gao and bretscher, 2010). Thus, inappropriate polar growth caused by loss of Gin4 could be due at least partly to misregulation of Bnr1. The fission yeast homolog of Gin4 also executes functions that are independent of Cdk1 inhibitory phosphorylation (Breeding *et al.*, 1998).

Growth-dependent signaling suggests a broadly relevant mechanism for control of cell growth and size

Theoretical analysis has shown that cell size control can be achieved by a mechanism in a constant increment of growth is added during each cell cycle that is independent of initial size (Campos *et al.*, 2014). This “adder” model for cell size control suggests that cells measure how much growth has occurred, rather than the absolute size of a cell. Adder behavior has been reported in cells ranging from bacteria to vertebrates, although the underlying molecular mechanisms have remained unknown (Campos *et al.*, 2014; Cadart *et al.*, 2018). Growth-dependent signaling suggests a mechanistic basis for adder behavior. Thus, delivery of anionic phospholipids could generate a signal that is proportional to the amount of phospholipid delivered to the growing membrane, which could be used to measure how much growth has occurred.

A previous study found evidence that growth-dependent signaling is also used to link mitotic entry to completion of the interval of polar bud growth (Anastasia *et al.*, 2012). In this case it was found that a member of the atypical protein kinase C family (Pkc1) undergoes gradual hyperphosphorylation that is dependent upon and proportional to polar bud growth. Once activated, Pkc1 relays signals that drive mitotic entry. Key signaling proteins in the Pkc1 axis are localized to the site of polar growth and physically interact (Drees et al., 2001; Yamochi et al., 1994; Andrews and Stark, 2000; Anastasia et al., 2012; Gentry and Hallberg, 2002; Rossio and Yoshida, 2011). Moreover, Pkc1 appears to play important functions in TORC2 signaling networks that control cell growth (Roelants *et al.*, 2017). Thus, growth-dependent control of Pkc1

shows strong similarities to the Gin4-related kinases but appears to influence the interval of polar growth that occurs before mitotic entry. There is some evidence that Pkc1 may also be responding to phosphatidylserine; however, a phosphatidylserine-binding domain in Pkc1 has not yet been rigorously defined (Nomura et al., 2017; Kamada et al., 1996).

Signals associated with plasma membrane growth also control ribosome biogenesis (Nanduri and Tartakoff, 2001; Mizuta and Warner, 1994). Thus, both of the core processes of growth – ribosome biogenesis and membrane growth – could be monitored and controlled via growth-dependent signals generated at the plasma membrane.

Is cell size an outcome of mechanisms that control cell growth?

In contrast to the adder model for size control, "sizer" models postulate that cells measure their size and delay cell cycle progression until a critical size has been reached (Jorgensen and Tyers, 2004b; Turner *et al.*, 2012; Ginzberg *et al.*, 2015). In sizer models, cells measure an outcome of growth (cell size) but otherwise have no mechanistic connection to the events of growth or to the signals that control cell growth. Yet there is increasing evidence for close mechanistic connections between cell growth and size. The discovery of growth-dependent signals that influence key cell cycle regulators suggests that the events of growth are translated into a proportional signal that is used to measure growth (Anastasia *et al.*, 2012). Furthermore, Gin4-related kinases and Pkc1, the key kinases known to be involved in growth-dependent signaling, also appear to play roles in controlling cell growth. For example, Gin4-related kinases control the pattern of growth and are also linked to the TORC2 network, which is thought to play a central role in control of cell growth. Thus, loss of Gin4-related kinases causes reduced TORC2 signaling, as well as defects in nutrient modulation of TORC2 signaling (Alcaide-Gavilan *et al.*, 2018). Conversely, mutants that are thought to cause increased TORC2-dependent signaling also cause increased phosphorylation of Gin4-related kinases (Zapata *et al.*, 2014; Lucena *et al.*, 2018). Similarly, Pkc1 has been linked to ribosome biogenesis, membrane trafficking, and organization of actin filaments (Roelants *et al.*, 2017).

Further evidence for a close relationship between control of cell growth and size has come from analysis of the relationship between growth rate and cell size. Studies in diverse cell types have found that growth rate is proportional to nutrient availability, cell size is proportional to growth rate, and growth rate is proportional to cell size (Leitao and Kellogg, 2017; Schmoller et al., 2015; Schaechter et al., 1958; Tzur et al., 2009; Sung et al., 2013; Cadart et al., 2018). In yeast, these proportional relationships are dependent upon the TORC2 signaling network (Lucena *et al.*, 2018). Analysis of the network suggests that TORC2-dependent signals that set growth rate also set the critical amount of growth required for cell cycle progression, which would point to a close relationship between cell size and the signals that control cell growth. There is also evidence that signals arising from ribosome biogenesis pathways influence cell size (Jorgensen and Tyers, 2004a; Jorgensen et al., 2002). It seems likely that the signals that control cell growth must ensure that the rates of membrane synthesis and ribosome biogenesis are matched to each other and to the growth rate set by nutrient availability. Thus, decreased rates of ribosome biogenesis or membrane growth might be expected to trigger a global decrease in growth rate as well as an associated decrease in cell size.

A general model that could explain these observations is that growth-dependent signals ensure that TORC2 signaling and growth rate scale with cell size, and that cell size scales with growth rate. Signals from the TORC2 network could influence cell size by setting the threshold level of Gin4 hyperphosphorylation required for cell cycle progression, which would effectively

match cell size to growth rate. Gin4-related kinases at the bud neck could function to define the boundaries of a domain of growth within the daughter bud, where they would be ideally positioned to report on the extent of bud growth, while also coordinating the events of growth.

From an evolutionary perspective, it would perhaps make sense that mechanisms that limit the extent of growth evolved in close association with the actual events of growth. In this view, cell size is an outcome of mechanisms that control cell growth, rather than the outcome of a mechanism that measures cell size independently of the molecular events that drive and control growth.

Materials and Methods

Yeast strain construction, media, and reagents

All strains are in the W303 background (*leu2-3,112 ura3-1 can1-100 ade2-1 his3-11,15 trp1-1 GAL+ ssd1-d2*). The additional genetic features of strains are listed in Table S1. Cells were grown in YP medium (1% yeast extract, 2% peptone, 40 mg/liter adenine) supplemented with 2% dextrose (YPD), or 2% glycerol and 2% ethanol (YPG/E). For live cell imaging, cells were grown in complete synthetic medium (CSM) supplemented with 2% dextrose and 40 mg/ml adenine.

Gene deletions and C-terminal epitope tagging was performed by standard PCR amplification and homologous recombination (Longtine *et al.*, 1998; Janke *et al.*, 2004; Lee *et al.*, 2013). *gin4-ΔKA1-LactC2* constructs integrated at the GIN4 locus were created by gene splicing with overlap extension (Horton *et al.*, 1990). Briefly, LactC2 fragments were PCR amplified from the plasmids pKT2100 or pKT1995 (Takeda *et al.*, 2014) with 40bp of flanking sequence at the 5' end that was homologous to the GIN4 ORF just upstream of the KA1 domain (amino acids 1007-1142) using oligos Gin4-39 and Gin4-40 (Table 2). The 3xHA::His3MX6 fragment was amplified from pFA6a-3HA-His3MX6 (Longtine *et al.*, 1998) with 5' homology to the terminal sequence of LactC2 and 3' homology to the DNA sequence just downstream of the Gin4 ORF using primers Gin4-38 and Gin4-41. The two fragments were then gel purified, annealed to each other and elongated for 15 PCR cycles in the absence of primers, followed by PCR amplification using primers Gin4-38 and Gin4-39. The resulting fragments were then transformed into wild type cells and correct integrants were identified by western blotting with anti-HA antibody. To create the GFP-tagged versions of the *gin4-ΔKA1-LactC2* constructs, GFP-His3MX6 was amplified from pFA6a-GFP-His3MX6 (Longtine *et al.*, 1998) and spliced to LactC2 as described above.

To generate strains with an AID tag on *GIN4* and/or *HSL1*, the *HSL1* gene was tagged at the C-terminus with an AID tag marked with KanMX6 in a parent strain that has two copies of the *TIR1* gene. The KanMX6 marker was then replaced by a *TRP1* marker. Next, a second AID tag marked with KanMX6 was incorporated at the *GIN4* locus. The *SPC42* gene in all four AID-tagged strains was fused to GFP at the C-terminus using standard PCR and homologous recombination. The parent strain that contains *2xTIR1* was used as the control strain and was modified to express endogenous SPC42 fused with yeast-optimized mRuby2 (yomRuby2). Auxin was dissolved in 100% ethanol to make a 50 mM stock solution.

Cell cycle time courses and Western blotting

Cell cycle time courses were carried out as previously described (Harvey *et al.*, 2011). Briefly, cells were grown to log phase at room temperature overnight in YPD or YPG/E to an optical density (OD_{600}) of 0.5 - 0.7. Cultures were adjusted to the same optical density and were then arrested in G1 phase by incubation in the presence of 0.5 µg/mL α factor at room temperature for 3 hours. Cells were released from the arrest by washing 3 times with fresh YPD or YPG/E. All time courses were carried out at 25˚C unless otherwise noted, and α factor was added back at 70 minutes to prevent initiation of a second cell cycle. For experiments involving auxin-mediated destruction of proteins, a single culture synchronized in G1 phase was split into two culture flasks and 0.5 mM auxin was added to one flask at 20 minutes after release from the G1 phase arrest. An equivalent volume of ethanol was added to the control flask.

For western blotting, 1.6 mL sample volumes were collected in screw cap tubes and centrifuged at 13,000 rpm for 30 sec. After discarding the supernatant, 200 µL acid washed glass

beads were added to the tubes and the samples were frozen in liquid nitrogen. Cells were lysed in 140 µL sample buffer (65 mM Tris HCl, pH-6.8, 3% SDS, 10% glycerol, 50 mM sodium fluoride, 100 mM ß-glycerophosphate, 5% ß-mercaptoethanol, and bromophenol blue) supplemented with 2 mM PMSF immediately before use. For experiments involving immunoblotting for Gin4-AID proteins, the sample buffer also included the protease cocktail LPC (1 mg/mL leupeptin, 1 mg/mL pepstatin, 1 mg/mL chymostatin dissolved in dimethylsulfoxide; used at 1/500 dilution). Sample buffer was added to cells immediately after they were removed from liquid nitrogen and the cells were then lysed in a Mini-beadbeater 16 (BioSpec) at top speed for 2 min. After a brief centrifugation, the samples were placed in a boiling water bath for 5 min and were then centrifuged again at 13,000 rpm for 3 min before loading onto SDS-PAGE gels. SDS PAGE was carried out as previously described (Harvey *et al.*, 2011). 10% polyacrylamide gels with 0.13% bis-acrylamide were used for analysis of Gin4, Clb2, and Nap1 (loading control). 9% polyacrylamide gels with 0.14% bis-acrylamide were used for Hsl1 and Swe1 blots. Proteins were immobilized onto nitrocellulose membranes using wet transfers for 1h 45 min. Blots were probed with the primary antibody at 1-2 µg/mL at room temperature overnight in 5% milk in PBST (1x phosphate buffered saline, 250 mM NaCl, 0.1% Tween-20) with 0.02% sodium azide. All the primary antibodies used in this study are rabbit polyclonal antibodies generated as described previously (Sreenivasan and Kellogg, 1999; Kellogg and Murray, 1995; Altman and Kellogg, 1997; Mortensen et al., 2002). Primary antibodies were detected by an HRP-conjugated donkey anti-rabbit secondary antibody (GE Healthcare; # NA934V) incubated in PBST for 1h at room temperature. Blots were rinsed in PBS before detection via chemiluminescence using ECL reagents (Advansta; #K-12045-D50) with a Bio-Rad ChemiDoc imaging system.

Coulter counter analysis

Cell cultures were grown in 10 mL YPD medium to an OD_{600} between 0.4 - 0.6. Cells were fixed by addition of 1/10 volume of 37% formaldehyde to the culture medium followed by incubation at room temperature for 1h. Cells were then pelleted and resuspended in 0.5 mL PBS containing 0.02% sodium azide and 0.1% Tween-20 and analyzed on the same day. Cell size was measured using a Coulter counter (Channelizer Z2; Beckman Coulter) as previously described (Jorgensen *et al.*, 2002; Artiles *et al.*, 2009). Briefly, 40 µL of fixed cells were diluted in 10 mL diluent (Isoton II; Beckman Coulter) and sonicated for 5 pulses of approximately 0.5 second each at low power. The Coulter Counter data shown in the figures represents the average of 3 biological replicates that is each the average of 3 technical replicates. For Fig. 6 C the strains were grown to log phase overnight at room temperature, diluted to OD_{600} - 0.1 in 5 mL fresh YPD, and then incubated for 4-5 h at 30˚C to observe temperature-dependent phenotypes of the mutants.

Microscopy

For DIC imaging, cells were grown to log phase in YPD and fixed in 3.7% formaldehyde for 30 min and then resuspended in PBS with 0.1% Tween-20 and 0.02% sodium azide. Images were obtained using a Zeiss-Axioskop 2 Plus microscope fitted with a 63x Plan-Apochromat 1.4 n.a. objective and an AxioCam HR camera (Carl Zeiss, Thornwood, NY). Images were acquired using AxioVision software and processed on Fiji (Schindelin *et al.*, 2012).

For live cell time-lapse imaging, the control strain (DK3510) and AID-tagged strains (DK3307, DK3308, DK3327 or DK3330) were grown in CSM overnight to an OD_{600} of 0.1 - 0.2 and then arrested in G1 phase with α factor. The control and the AID-tagged strains were mixed

in a 1.6 mL tube and then washed 3X in CSM prewarmed to 30˚C to release the cells from the G1 phase arrest. After resuspending the cells in CSM, approximately 200 µL cells were immobilized onto a concanavalin A-treated chambered #1.5 Coverglass system (Labtek-II; Nunc™#155409) for 5 min. Unbound cells were washed away by repeated washes with CSM. The cells were then incubated in 500 µL CSM at 27˚C for the duration of the imaging. Auxin was added to the cells to a final concentration of 0.5 mM 20 minutes after the first wash used to release the cells from the α factor arrest.

Scanning confocal images were acquired on a Zeiss 880 confocal microscope running ZEN Black software using a 63x/1.4 n.a. Plan Apo objective. The microscope was equipped with a heat block stage insert with a closed lid and exterior chamber for temperature control. The microscope was allowed to equilibrate at the set temperature of 27˚C for at least 1h to ensure temperature stability prior to imaging. Definite Focus was used to keep the sample in focus during the duration of the experiment. 1 x 2 tiled *z*-stack images were acquired every 3 min. Zoom and frame size were set to 0.8x magnification to achieve a consistent pixel area of 1024 x 1024 pixels in XY and pixel dwell time was 0.5 µs. Optical sections were taken for a total of 14 *z*-planes every 0.37 µm with frame averaging set to 2, to reduce noise. 488 nm laser power was set to 0.2 % and the 561 nm laser power was set to 1% to minimize cell damage. The gain for GFP, RFP and bright field was set to 550, 750 and 325, respectively. The same gain settings were used for each experiment. GFP signal was acquired on a GaAsP detector and collected between 498 nm - 548 nm. Brightfield images were collected simultaneously. RFP signal was acquired on a GaAsP detector and collected between 577 nm - 629 nm.

To visualize the localization of Gin4 constructs fused to GFP, cells were grown in CSM overnight, fixed in 3.7% formaldehyde for 15 min, and then resuspended in 500 µL 1x PBST. Images were acquired on a spinning disk confocal microscope with a Solamere system running MicroManager* (Edelstein *et al.*, 2014). The microscope was based on a Nikon TE2000 stand and Coherent OBIS lasers. We used a 100x/1.4 n.a. Plan Apo objective for Fig. 6 E and a 63x/1.4 Plan Apo objective for data collection in **Fig. S4**. Pixel sizes were 0.11 µm in X,Y and *z*-stack spacing was set to 0.5 µm with a total of 17 *z*-slices. GFP was excited at 488 nm and collected through a 525/50nm band pass filter (Chroma) onto a Hamamatsu ImageEMX2 EMCCD camera. Gain levels were set to 200 to maximize signal without hitting saturation. GFP and brightfield images were collected sequentially.

Image analysis

All images were analyzed on Fiji (Schindelin *et al.*, 2012). For visualization of GFP-tagged Gin4 constructs, a sum projection of *z*-slices was used. Movies for the time-lapse were processed as previously described (Leitao *et al.*, 2018). The bright field images were processed using the "Find Focused Slices" plugin available on Fiji to create a stack with the focused slice +/- one slice for each timepoint. A *z*-projection with sum of slices was performed on this stack and then bud volumes were determined using the plugin BudJ (Ferrezuelo *et al.*, 2012).

The timings of cell cycle events were determined as previously reported (Leitao and Kellogg, 2017). Briefly, bud initiation was manually determined by the appearance of a protrusion on the surface of the mother cell. The initiation of metaphase was marked by the appearance of separation of spindle poles to 2-3 microns apart. Initiation of anaphase was marked by further separation of the spindle poles and segregation of one of the poles into the daughter cell. We defined completion of anaphase as the point at which the spindle poles reached their maximal distance apart.

For a quantitative comparison of the localization of GFP-tagged Gin4 constructs in **Fig. S4**, a *z*-projection with sum of slices was performed on the images and an elliptical ROI was drawn around the bud neck. The maximum pixel intensity was determined for each cell after subtracting the background pixel intensity.

Statistical analysis

Data acquired from the image analysis were plotted as scatter dot plots using GraphPad Prism. The scatter plots show the data distribution along with the mean and standard deviation for each strain. For all scatter dot plots, the unpaired t-test was calculated using the Mann-Whitney test for non-Gaussian distributions and the two-tailed *p*-values have been mentioned.

Online supplemental material

Fig. S1 relates to Fig. 3 and provides a characterization of the *gin4-AID* and *hsl1-AID alleles.* Fig. S2 relates to Fig. 4 and shows further evidence for the role of Gin4 and Hsl1 in the control of bud growth. Fig. S3 relates to Fig. 5 and shows a time-dependent increase in the *gin4-AID hsl1-AID* phenotype. Fig. S4 relates to Fig. 6 and shows peak pixel intensity of the various Gin4-GFP constructs localized to the bud neck. Video 1 and Video 2 show time-lapse videos of *2xTIR1* and *gin4-AID hsl1-AID* cells as they progress through the cell cycle. The tables show yeast strains (Table 1), primers (Table 2), and plasmids (Table 3) used in this study.

Acknowledgements

We thank Ben Abrams and the UCSC Life Microscopy Facility for assistance with microscopy, Kazuma Tanaka, Thomas Eng and Doug Koshland for plasmids, and members of the laboratory for support and helpful advice. The authors declare no competing financial interests.

References

Alcaide-Gavilan, M., R. Lucena, K.A. Schubert, K.L. Artiles, J. Zapata, and D.R. Kellogg. 2018. Modulation of TORC2 Signaling by a Conserved Lkb1 Signaling Axis in Budding Yeast. *Genetics*. 210:155–170. doi:10.1534/genetics.118.301296.

Altman, R., and D. Kellogg. 1997. Control of mitotic events by Nap1 and the Gin4 kinase. *The Journal of Cell Biology*. 138:119–130.

Anastasia, S.D., D.L. Nguyen, V. Thai, M. Meloy, T. Macdonough, and D.R. Kellogg. 2012. A link between mitotic entry and membrane growth suggests a novel model for cell size control. *The Journal of Cell Biology*. 197:89–104. doi:10.1083/jcb.201108108.

Andrews, P.D., and M.J. Stark. 2000. Dynamic, Rho1p-dependent localization of Pkc1p to sites of polarized growth. *Journal of Cell Science*. 113 (Pt 15):2685–2693.

Artiles, K., S. Anastasia, D. McCusker, and D.R. Kellogg. 2009. The Rts1 regulatory subunit of protein phosphatase 2A is required for control of G1 cyclin transcription and nutrient modulation of cell size. *PLoS Genet*. 5:e1000727. doi:10.1371/journal.pgen.1000727.

Barral, Y., M. Parra, S. Bidlingmaier, and M. Snyder. 1999. Nim1-related kinases coordinate cell cycle progression with the organization of the peripheral cytoskeleton in yeast. *Genes & Development*. 13:176–187.

Bean, J.M., E.D. Siggia, and F.R. Cross. 2006. Coherence and Timing of Cell Cycle Start Examined at Single-Cell Resolution. *Molecular Cell*. 21:3–14. doi:10.1016/j.molcel.2005.10.035.

Breeding, C.S., J. Hudson, M.K. Balasubramanian, S.M. Hemmingsen, P.G. Young, and K.L. Gould. 1998. The cdr2(+) gene encodes a regulator of G2/M progression and cytokinesis in Schizosaccharomyces pombe. *Mol. Biol. Cell*. 9:3399–3415.

Buttery, S.M., K. Kono, E. Stokasimov, and D. Pellman. 2012. Regulation of the formin Bnr1 by septins anda MARK/Par1-family septin-associated kinase. *Mol. Biol. Cell*. 23:4041–4053. doi:10.1091/mbc.E12-05-0395.

Cadart, C., S. Monnier, J. Grilli, P.J. Sáez, N. Srivastava, R. Attia, E. Terriac, B. Baum, M. Cosentino-Lagomarsino, and M. Piel. 2018. Size control in mammalian cells involves modulation of both growth rate and cell cycle duration. *Nature Communications*. 9:3275. doi:10.1038/s41467-018-05393-0.

Campos, M., I.V. Surovtsev, S. Kato, A. Paintdakhi, B. Beltran, S.E. Ebmeier, and C. Jacobs-Wagner. 2014. A constant size extension drives bacterial cell size homeostasis. *Cell*. 159:1433–1446. doi:10.1016/j.cell.2014.11.022.

Carroll, C.W., R. Altman, D. Schieltz, J.R. Yates, and D. Kellogg. 1998. The septins are required for the mitosis-specific activation of the Gin4 kinase. *The Journal of Cell Biology*. 143:709–717.

Coleman, T.R., Z. Tang, and W.G. Dunphy. 1993. Negative regulation of the wee1 protein kinase by direct action of the nim1/cdr1 mitotic inducer. *Cell*. 72:919–929.

Drees, B.L., B. Sundin, E. Brazeau, J.P. Caviston, G.C. Chen, W. Guo, K.G. Kozminski, M.W. Lau, J.J. Moskow, A. Tong, L.R. Schenkman, A. McKenzie, P. Brennwald, M. Longtine, E. Bi, C. Chan, P. Novick, C. Boone, J.R. Pringle, T.N. Davis, S. Fields, and D.G. Drubin. 2001. A protein interaction map for cell polarity development. *The Journal of Cell Biology*. 154:549–571. doi:10.1083/jcb.200104057.

Edelstein, A.D., M.A. Tsuchida, N. Amodaj, H. Pinkard, R.D. Vale, and N. Stuurman. 2014. Advanced methods of microscope control using μManager software. *J Biol Methods*. 1:10. doi:10.14440/jbm.2014.36.

Ejsing, C.S., J.L. Sampaio, V. Surendranath, E. Duchoslav, K. Ekroos, R.W. Klemm, K. Simons, and A. Shevchenko. 2009. Global analysis of the yeast lipidome by quantitative shotgun mass spectrometry. *Proc. Natl. Acad. Sci. U.S.A.* 106:2136–2141. doi:10.1073/pnas.0811700106.

Fairn, G.D., M. Hermansson, P. Somerharju, and S. Grinstein. 2011. Phosphatidylserine is polarized and required for proper Cdc42 localization and for development of cell polarity. *Nat Cell Biol*. 13:1424–1430. doi:10.1038/ncb2351.

Ferrezuelo, F., N. Colomina, A. Palmisano, E. Garí, C. Gallego, A. Csikász-Nagy, and M. Aldea. 2012. The critical size is set at a single-cell level by growth rate to attain homeostasis and adaptation. *Nature Communications*. 3:1012. doi:10.1038/ncomms2015.

Finnigan, G.C., S.M. Sterling, A. Duvalyan, E.N. Liao, A. Sargsyan, G. Garcia, E. Nogales, and J. Thorner. 2016. Coordinate action of distinct sequence elements localizes checkpoint kinase Hsl1 to the septin collar at the bud neck in Saccharomyces cerevisiae. *Mol. Biol. Cell*. 27:2213–2233. doi:10.1091/mbc.E16-03-0177.

Fraschini, R., C. D'Ambrosio, M. Venturetti, G. Lucchini, and S. Piatti. 2006. Disappearance of the budding yeast Bub2-Bfa1 complex from the mother-bound spindle pole contributes to mitotic exit. *The Journal of Cell Biology*. 172:335–346. doi:10.1083/jcb.200507162.

Gao, and A. bretscher. 2010. The Yeast Formin Bnr1p Has Two Localization Regions That Show Spatially and Temporally Distinct Association with Septin Structures. 1–10. doi:10.1091/mbc.E09.

Gentry, M.S., and R.L. Hallberg. 2002. Localization of Saccharomyces cerevisiae protein phosphatase 2A subunits throughout mitotic cell cycle. *Mol. Biol. Cell*. 13:3477–3492. doi:10.1091/mbc.02-05-0065.

Ginzberg, M.B., R. Kafri, and M. Kirschner. 2015. On being the right (cell) size. *Science*. 348:1245075–1245075. doi:10.1126/science.1245075.

Grava, S., F. Schaerer, M. Faty, P. Philippsen, and Y. Barral. 2006. Asymmetric recruitment of dynein to spindle poles and microtubules promotes proper spindle orientation in yeast. *Dev Cell*. 10:425–439. doi:10.1016/j.devcel.2006.02.018.

Hartwell, L.H., and M.W. Unger. 1977. Unequal division in Saccharomyces cerevisiae and its implications for the control of cell division. *The Journal of Cell Biology*. 75:422–435.

Harvey, S.L., A. Charlet, W. Haas, S.P. Gygi, and D.R. Kellogg. 2005. Cdk1-dependent regulation of the mitotic inhibitor Wee1. *Cell*. 122:407–420. doi:10.1016/j.cell.2005.05.029.

Harvey, S.L., and D.R. Kellogg. 2003. Conservation of mechanisms controlling entry into mitosis: budding yeast wee1 delays entry into mitosis and is required for cell size control. *Current Biology*. 13:264–275.

Harvey, S.L., G. Enciso, N. Dephoure, S.P. Gygi, J. Gunawardena, and D.R. Kellogg. 2011. A phosphatase threshold sets the level of Cdk1 activity in early mitosis in budding yeast. *Mol. Biol. Cell*. 22:3595–3608. doi:10.1091/mbc.E11-04-0340.

Haupt, A., and N. Minc. 2017. Gradients of phosphatidylserine contribute to plasma membrane charge localization and cell polarity in fission yeast. *Mol. Biol. Cell*. 28:210–220. doi:10.1091/mbc.E16-06-0353.

Hikiji, T., K. Miura, K. Kiyono, I. Shibuya, and A. Ohta. 1988. Disruption of the CHO1 gene encoding phosphatidylserine synthase in Saccharomyces cerevisiae. *J. Biochem.* 104:894–900.

Horton, R.M., Z.L. Cai, S.N. Ho, and L.R. Pease. 1990. Gene splicing by overlap extension: tailor-made genes using the polymerase chain reaction. *Biotech.* 8:528–535.

Johnston, G.C., C.W. Ehrhardt, A. Lorincz, and B.L. Carter. 1979. Regulation of cell size in the yeast Saccharomyces cerevisiae. *J. Bacteriol.* 137:1–5.

Johnston, G.C., J.R. Pringle, and L.H. Hartwell. 1977. Coordination of growth with cell division in the yeast Saccharomyces cerevisiae. *Exp. Cell Res.* 105:79–98.

Jorgensen, P., and M. Tyers. 2004a. A dynamic transcriptional network communicates growth potential to ribosome synthesis and critical cell size. *Genes & Development*. 18:2491–2505. doi:10.1101/gad.1228804.

Jorgensen, P., and M. Tyers. 2004b. How Cells Coordinate Growth and Division. *Current Biology*. 14:R1014–R1027. doi:10.1016/j.cub.2004.11.027.

Jorgensen, P., J.L. Nishikawa, B.-J. Breitkreutz, and M. Tyers. 2002. Systematic identification of pathways that couple cell growth and division in yeast. *Science*. 297:395–400. doi:10.1126/science.1070850.

Kamada, Y., H. Qadota, C.P. Python, Y. Anraku, Y. Ohya, and D.E. Levin. 1996. Activation of yeast protein kinase C by Rho1 GTPase. *J. Biol. Chem.* 271:9193–9196.

Kanoh, J., and P. Russell. 1998. The protein kinase Cdr2, related to Nim1/Cdr1 mitotic inducer, regulates the onset of mitosis in fission yeast. *Mol. Biol. Cell*. 9:3321–3334.

Kellogg, D.R., and A.W. Murray. 1995. NAP1 acts with Clb2 to perform mitotic functions and to suppress polar bud growth in budding yeast. *The Journal of Cell Biology*. 130:675–685.

Klose, C., M.A. Surma, M.J. Gerl, F. Meyenhofer, A. Shevchenko, and K. Simons. 2012. Flexibility of a eukaryotic lipidome--insights from yeast lipidomics. *PLoS ONE*. 7:e35063. doi:10.1371/journal.pone.0035063.

Klug, L., and G. Daum. 2014. Yeast lipid metabolism at a glance. *FEMS Yeast Res*. 14:369–388. doi:10.1111/1567-1364.12141.

Lee, S., W.A. Lim, and K.S. Thorn. 2013. Improved Blue, Green, and Red Fluorescent Protein Tagging Vectors for S. cerevisiae. *PLoS ONE*. 8:e67902. doi:10.1371/journal.pone.0067902.s007.

Leitao, R.M., and D.R. Kellogg. 2017. The duration of mitosis and daughter cell size are modulated by nutrients in budding yeast. *The Journal of Cell Biology*. 216:3463–3470. doi:10.1083/jcb.201609114.

Leitao, R.M.M., A. Pham, Q. Okobi, and D. Kellogg. 2018. PP2A-Rts1 enforces a proportional relationship between cell size and growth rate. *bioRxiv*. 1–28. doi:10.1101/321281.

Lew, D.J., and S.I. Reed. 1993. Morphogenesis in the yeast cell cycle: regulation by Cdc28 and cyclins. *The Journal of Cell Biology*. 120:1305–1320.

Longtine, M.S., A. McKenzie, D.J. DeMarini, N.G. Shah, A. Wach, A. Brachat, P. Philippsen, and J.R. Pringle. 1998. Additional modules for versatile and economical PCR-based gene deletion and modification in Saccharomyces cerevisiae. *Yeast*. 14:953–961. doi:10.1002/(SICI)1097-0061(199807)14:10<953::AID-YEA293>3.0.CO;2-U.

Longtine, M.S., C.L. Theesfeld, J.N. McMillan, E. Weaver, J.R. Pringle, and D.J. Lew. 2000. Septin-Dependent Assembly of a Cell Cycle-Regulatory Module in Saccharomyces cerevisiae. *Molecular and Cellular Biology*. 20:4049–4061. doi:10.1128/MCB.20.11.4049-4061.2000.

Lucena, R., M. Alcaide-Gavilan, K. Schubert, M. He, M.G. Domnauer, C. Marquer, C. Klose, M.A. Surma, and D.R. Kellogg. 2018. Cell Size and Growth Rate Are Modulated by TORC2-Dependent Signals. *Curr. Biol.* 28:196–210.e4. doi:10.1016/j.cub.2017.11.069.

Ma, X.J., Q. Lu, and M. Grunstein. 1996a. A search for proteins that interact genetically with histone H3 and H4 amino termini uncovers novel regulators of the Swe1 kinase in Saccharomyces cerevisiae. *Genes & Development*. 10:1327–1340. doi:10.1101/gad.10.11.1327.

Ma, X.J., Q. Lu, and M. Grunstein. 1996b. A search for proteins that interact genetically with histone H3 and H4 amino termini uncovers novel regulators of the Swe1 kinase in Saccharomyces cerevisiae. *Genes & Development*. 10:1327–1340.

Matsuo, Y., E. Fisher, J. Patton-Vogt, and S. Marcus. 2007. Functional Characterization of the Fission Yeast Phosphatidylserine Synthase Gene, pps1, Reveals Novel Cellular Functions for Phosphatidylserine. *Eukaryotic Cell*. 6:2092–2101. doi:10.1128/EC.00300-07.

McCusker, D., C. Denison, S. Anderson, T.A. Egelhofer, J.R. Yates, S.P. Gygi, and D.R. Kellogg. 2007. Cdk1 coordinates cell-surface growth with the cell cycle. *Nat Cell Biol*. 9:506–515. doi:10.1038/ncb1568.

Mizuta, K., and J.R. Warner. 1994. Continued functioning of the secretory pathway is essential for ribosome synthesis. *Molecular and Cellular Biology*. 14:2493–2502.

Moravcevic, K., J.M. Mendrola, K.R. Schmitz, Y.-H. Wang, D. Slochower, P.A. Janmey, and M.A. Lemmon. 2010. Kinase Associated-1 Domains Drive MARK/PAR1 Kinases to Membrane Targets by Binding Acidic Phospholipids. *Cell*. 143:966–977. doi:10.1016/j.cell.2010.11.028.

Mortensen, E.M., H. McDonald, J. Yates, and D.R. Kellogg. 2002. Cell cycle-dependent assembly of a Gin4-septin complex. *Mol. Biol. Cell*. 13:2091–2105. doi:10.1091/mbc.01-10-0500.

Nanduri, J., and A.M. Tartakoff. 2001. The arrest of secretion response in yeast: signaling from the secretory path to the nucleus via Wsc proteins and Pkc1p. *Molecular Cell*. 8:281–289.

Nishimura, K., T. Fukagawa, H. Takisawa, T. Kakimoto, and M. Kanemaki. 2009. An auxin-based degron system for the rapid depletion of proteins in nonplant cells. *Nat Meth*. 6:917–922. doi:10.1038/nmeth.1401.

Nomura, W., Y. Ito, and Y. Inoue. 2017. Role of phosphatidylserine in the activation of Rho1-related Pkc1 signaling in Saccharomyces cerevisiae. *Cellular Signalling*. 31:146–153. doi:10.1016/j.cellsig.2017.01.002.

Okuzaki, D., S. Tanaka, H. Kanazawa, and H. Nojima. 1997. Gin4 of S. cerevisiae is a bud neck protein that interacts with the Cdc28 complex. *Genes Cells*. 2:753–770.

Pruyne, D., L. Gao, E. Bi, and A. Bretscher. 2004. Stable and dynamic axes of polarity use distinct formin isoforms in budding yeast. *Mol. Biol. Cell*. 15:4971–4989. doi:10.1091/mbc.E04-04-0296.

Raspelli, E., C. Cassani, G. Lucchini, and R. Fraschini. 2011. Budding yeast Dma1 and Dma2 participate in regulation of Swe1 levels and localization. *Mol. Biol. Cell*. 22:2185–2197. doi:10.1091/mbc.E11-02-0127.

Roelants, F.M., K.L. Leskoske, M.N. Martinez Marshall, M.N. Locke, and J. Thorner. 2017. The TORC2-Dependent Signaling Network in the Yeast Saccharomyces cerevisiae. *Biomolecules*. 7. doi:10.3390/biom7030066.

Rossio, V., and S. Yoshida. 2011. Spatial regulation of Cdc55-PP2A by Zds1/Zds2 controls mitotic entry and mitotic exit in budding yeast. *The Journal of Cell Biology*. 193:445–454. doi:10.1083/jcb.201101134.

Schaechter, M., O. Maaloe, and N.O. Kjeldgaard. 1958. Dependency on medium and temperature of cell size and chemical composition during balanced grown of Salmonella typhimurium. *J. Gen. Microbiol.* 19:592–606. doi:10.1099/00221287-19-3-592.

Schindelin, J., I. Arganda-Carreras, E. Frise, V. Kaynig, M. Longair, T. Pietzsch, S. Preibisch, C. Rueden, S. Saalfeld, B. Schmid, J.-Y. Tinevez, D.J. White, V. Hartenstein, K. Eliceiri, P. Tomancak, and A. Cardona. 2012. Fiji: an open-source platform for biological-image analysis. *Nat Meth*. 9:676–682. doi:10.1038/nmeth.2019.

Schmoller, K.M., J.J. Turner, M. Kõivomägi, and J.M. Skotheim. 2015. Dilution of the cell cycle inhibitor Whi5 controls budding-yeast cell size. *Nature*. doi:10.1038/nature14908.

Shao, C., V.A. Novakovic, J.F. Head, B.A. Seaton, and G.E. Gilbert. 2008. Crystal structure of lactadherin C2 domain at 1.7A resolution with mutational and computational analyses of its membrane-binding motif. *Journal of Biological Chemistry*. 283:7230–7241. doi:10.1074/jbc.M705195200.

Shulewitz, M.J., C.J. Inouye, and J. Thorner. 1999. Hsl7 localizes to a septin ring and serves as an adapter in a regulatory pathway that relieves tyrosine phosphorylation of Cdc28 protein kinase in Saccharomyces cerevisiae. *Molecular and Cellular Biology*. 19:7123–7137.

Sreenivasan, A., A.C. Bishop, K.M. Shokat, and D.R. Kellogg. 2003. Specific inhibition of Elm1 kinase activity reveals functions required for early G1 events. *Molecular and Cellular Biology*. 23:6327–6337. doi:10.1128/MCB.23.17.6327–6337.2003.

Sreenivasan, A., and D. Kellogg. 1999. The elm1 kinase functions in a mitotic signaling network in budding yeast. *Molecular and Cellular Biology*. 19:7983–7994.

Sung, Y., A. Tzur, S. Oh, W. Choi, V. Li, R.R. Dasari, Z. Yaqoob, and M.W. Kirschner. 2013. Size homeostasis in adherent cells studied by synthetic phase microscopy. *Proc. Natl. Acad. Sci. U.S.A.* 110:16687–16692. doi:10.1073/pnas.1315290110.

Takeda, M., K. Yamagami, and K. Tanaka. 2014. Role of Phosphatidylserine in Phospholipid Flippase-Mediated Vesicle Transport in Saccharomyces cerevisiae. *Eukaryotic Cell*. 13:363–375. doi:10.1128/EC.00279-13.

Thornton, B.R., and D.P. Toczyski. 2003. Securin and B-cyclin/CDK are the only essential targets of the APC. *Nat Cell Biol*. 5:1090–1094. doi:10.1038/ncb1066.

Turner, J.J., J.C. Ewald, and J.M. Skotheim. 2012. Cell size control in yeast. *Curr. Biol.* 22:R350–9. doi:10.1016/j.cub.2012.02.041.

Tzur, A., R. Kafri, V.S. LeBleu, G. Lahav, and M.W. Kirschner. 2009. Cell Growth and Size Homeostasis in Proliferating Animal Cells. *Science*. 325:167–171. doi:10.1126/science.1174294.

Yamochi, W., K. Tanaka, H. Nonaka, A. Maeda, T. Musha, and Y. Takai. 1994. Growth site localization of Rho1 small GTP-binding protein and its involvement in bud formation in Saccharomyces cerevisiae. *The Journal of Cell Biology*. 125:1077–1093.

Yeung, T., G.E. Gilbert, J. Shi, J. Silvius, A. Kapus, and S. Grinstein. 2008. Membrane Phosphatidylserine Regulates Surface Charge and Protein Localization. *Science*. 319:210–213. doi:10.1126/science.1152066.

Young, P.G., and P.A. Fantes. 1987. Schizosaccharomyces pombe mutants affected in their division response to starvation. *Journal of Cell Science*. 88 (Pt 3):295–304.

Zapata, J., N. Dephoure, T. Macdonough, Y. Yu, E.J. Parnell, M. Mooring, S.P. Gygi, D.J. Stillman, and D.R. Kellogg. 2014. PP2ARts1 is a master regulator of pathways that control cell size. *The Journal of Cell Biology*. 204:359–376. doi:10.1083/jcb.201309119.

Figure legends

Figure 1: Hyperphosphorylation of Gin4 and Hsl1 is proportional to the extent of bud growth.
Wild type cells grown overnight in YPD **(A)** or YPG/E **(B)** were arrested with α factor. The cells were then released from the arrest at 25˚C and samples were taken at 10 min intervals. The behavior of Gin4, Hsl1-6XHA and Clb2 was assayed by western blot. **(C)** A direct comparison of the maximal extent of Gin4 phosphorylation in rich or poor carbon was made by comparing samples taken at peak Clb2 expression in each condition (90 min in rich carbon and 140 min in poor carbon). An anti-Nap1 antibody was used as a loading control.

Figure 2: Hyperphosphorylation of Gin4 is dependent upon bud growth.
Wild type, *swe1*Δ and *swe1*Δ *sec6-4* cells were released from a G1 arrest in YPD at room temperature and shifted to the restrictive temperature (34˚C) 30 min after release from arrest. Samples were taken at the indicated intervals and the behavior of Gin4 **(A)** and Clb2 **(B)** was analyzed by western blot. **(C)** A direct comparison of the extent of Gin4 phosphorylation was made by loading samples from all three strains taken at 90 min (wild type), 80 min (*swe1*Δ) and 100 min (*sec6-4 swe1*Δ).

Figure 3: Gin4 and Hsl1 are required for normal control of cell growth and size in mitosis.
(A) Control cells and *gin4-AID hsl1-AID* cells growing in YPD were released from a G1 arrest at 25˚C and 0.5 mM auxin was added to both strains 20 min after release. Both strains included 2 copies of the *TIR1* gene. Samples were taken at the indicated intervals and the behavior of Swe1 and Clb2 was analyzed by western blot. **(B)** Control cells and *gin4-AID hsl1-AID* cells were differentially marked with fluorescently-tagged mitotic spindle poles. Thus, control cells express *SPC42-mRuby2*. while the *gin4-AID hsl1-AID* cells express *SPC42-GFP*. Both strains include 2 copies of the *TIR1* gene. Cells growing in CSM were arrested with α factor and then mixed together before releasing from the arrest. Auxin was added to 0.5 mM at 20 minutes after release from arrest, which corresponds to approximately 30 minutes before bud emergence. Cells were then imaged at 3-minute intervals by confocal microscopy at 27°C. Bud emergence was used to set the zero timepoint. Key mitotic transitions are highlighted for each strain.

Figure 4: Gin4 and Hsl1 are required for normal control of cell growth and size in mitosis.
Cells of the indicated genotypes were released from a G1 arrest and analyzed by confocal microscopy as described for Fig. 3 B. All strains included 2 copies of the *TIR1* gene. **(A)** Scatter plots showing the duration of metaphase and anaphase. **(B)** Scatter plots showing bud size at completion of metaphase and anaphase. **(C)** Plots showing cell size at completion of mitosis versus growth rate in mitosis for control cells and *gin4-AID hsl1-AID* cells. **(D)** Scatter plots showing the ratio of major axis to minor axis of the bud at completion of anaphase. For panels **A,B,D**, the mean and standard deviation for each strain are shown.

Figure 5: Gin4 and Hsl1 are required for normal control of mother cell growth
Cells of the indicated genotypes were released from a G1 arrest and analyzed by confocal microscopy as described for Fig. 3 B. **(A)** A representative plot of mother and daughter cell size as a function of time. In each case, the daughter cell is the daughter of the mother cell shown in the same plot. **(B)** Scatter plots showing the net increase in mother cell volume from the time of

bud emergence to completion of anaphase. The plot shows the mean and standard deviation for each strain.

Figure 6: Proportional phosphorylation of Gin4 during bud growth requires binding to anionic phospholipids

Cells of the indicated genotypes were released from a G1 arrest in YPD at 30˚C. The behavior of Gin4 **(A)** and Clb2 **(B)** was analyzed by western blot. In each strain, Gin4 constructs were marked with a 3xHA tag and detected with anti-HA antibody. The signal for *gin4-ΔKA1* and the LactC2 constructs was weaker, so these blots were exposed longer. Gin4-ΔKA1-3xHA was about 16 KDa smaller than the other proteins. **(C)** Cells of the indicated genotypes were grown in YPD overnight, diluted in fresh YPD, and then incubated for 5h at 30˚C. The size distribution for each strain was analyzed using a Coulter counter. **(D)** Cells of the indicated genotypes were grown to log phase in YPD at 25˚C and imaged by DIC optics. **(E)** Cellular localization of Gin4, Gin4-ΔKA1, Gin4-ΔKA1-LactC2 and Gin4-ΔKA1-LactC2^{AAA} fused to GFP at the C-terminus. All four strains were excited by the GFP-laser with identical settings at 100x magnification and displayed with the same brightness levels to compare relative levels of Gin4 localized to the bud neck. Gin4-ΔKA1-GFP shows mostly cytoplasmic localization with a small level of bud neck localization (white arrowheads). The brightfield images for each field are shown below. Scale bar represents 5 µm.

Figure S1: Characterization of *gin4-AID* and *hsl1-AID* alleles

(A) Wild type, *2xTIR1* control cells*, gin4-AID hsl1-AID 2xTIR1 cells* and *gin4-AID hsl1-AID swe1Δ 2xTIR1* cells were grown overnight at room temperature in YPD and cell size distributions were analyzed with a Coulter counter. **(B)** Control cells and *gin4-AID hsl1-AID* cells growing in YPD were released from a G1 phase arrest. After release, the *gin4-AID hsl1-AID* cells were split into two aliquots and 0.5 mM auxin was added to one aliquot and an equivalent amount of the solvent for auxin was added to the other. Auxin was also added to the control strain. Samples were taken at the indicated intervals and the behavior of Gin4 was analyzed by western blot. All strains contain 2 copies of the *TIR1* gene (*2xTIR1*). **(C)** *gin4-AID hsl1-AID 2xTIR1* cells growing in YPD were released from a G1 phase arrest. After release, the cells were split into two aliquots and 0.5 mM auxin was added to one aliquot and an equivalent amount of the solvent for auxin was added to the other. Samples were taken at the indicated intervals and the behavior of Clb2 was analyzed by western blot. **(D)** *gin4-AID hsl1-AID 2xTIR1* cells were grown to log phase in YPD and were then split into two aliquots. 0.5 mM auxin was added to one aliquot and an equivalent amount of the solvent for auxin was added to the other. Samples were taken at the indicated intervals and the behavior of Swe1 was analyzed by western blot. Anti-Nap1 was used as loading control.

Figure S2: Gin4 and Hsl1 control bud growth during mitosis

(A) *gin4Δ, hsl1Δ, gin4Δ hsl1Δ, and gin4Δ hsl1Δ swe1Δ* cells were grown to log phase in YPD media at 25˚C and images were obtained using DIC optics. **(B)** A scatter plot showing the growth rate of the daughter buds during mitosis for the indicated genotypes. The growth rate (fL/min) was determined as the increase in bud volume from initiation of metaphase to the completion of anaphase, divided by the total time spent in metaphase and anaphase.

Figure S3: The severity of the *gin4-AID hsl1-AID* phenotype increases with time.

Control cells and *gin4-AID hsl1-AID* cells were grown to log phase at room temperature in YPD medium and auxin was added to both strains. Both strains included 2 copies of the *TIR1* gene. DIC images of the cells were taken at the indicated times. Scale bar represents 5 µm.

Figure S4: Quantification of Gin4-GFP constructs at the bud neck.
Cells of the indicated genotypes were analyzed to determine the maximum pixel intensity for GFP fluorescence at the bud neck. The Y-axis on the scatter plot shows the maximum pixel intensity in arbitrary units after subtracting background signal.

Video 1: Time-lapse imaging of *2xTIR1* and *gin4-AID hsl1-AID* cells.
The two strains were mixed together prior to imaging as described in Materials and methods. The spindle pole bodies were differentially tagged in the two strains. The cells in top right corner show *2xTIR1* cells with mRuby2-tagged SPC42 and the cells in the bottom left corner show *gin4-AID hsl1-AID* with GFP-tagged SPC42. The *gin4-AID hsl1-AID* cells undergo a prolonged metaphase delay with polarized bud growth while the *2xTIR1* cells begin the next cell cycle. The cells were imaged using time-lapse confocal microscopy with image acquisition every 3 min. The movie was converted to AVI format using Fiji and shows the time-lapse at a speed of 5 frames per second (fps). Scale bar represents 5 µm.

Video 2: *gin4-AID hsl1-AID* cells show spindle pole and cytokinesis defects.
A tile showing *2xTIR1* cells with mRuby2-tagged SPC42 and *gin4-AID hsl1-AID* cells with GFP-tagged SPC42 imaged together. Cells were imaged using time-lapse confocal microscopy with image acquisition every 3 min. The *gin4-AID hsl1-AID* cells exhibit defects in bud separation and results in the formation of cell chains. These defects are also accompanied by spindle defects (magenta arrows) in the second cell cycle. The movie was converted to AVI format using Fiji and shows the time-lapse at a speed of 5 fps.

Table 1: Strains used in this study

Strain	Mating type	Genotype	Source
DK 186	a	*bar1Δ*	(Altman and Kellogg, 1997)
DK 3418	a	*bar1Δ HSL1-6XHA::His3MX6*	This study
SH 24	a	*bar1Δ swe1Δ::URA3*	(Harvey and Kellogg, 2003)
DK 1600	a	*bar1Δ swe1Δ::His3MX6 sec6-4::KanMX6*	(Anastasia *et al.*, 2012)
DK 3510	a	*bar1Δ his3::His3MX6+TIR1 leu2::LEU2+TIR1 SPC42-yomRuby2::KanMX6*	This study
DK 3307	a	*bar1Δ his3::His3MX6+TIR1 leu2::LEU2+TIR1 SPC42-GFP::HphNTI gin4-AID::KanMX6*	This study
DK 3308	a	*bar1Δ his3::His3MX6+TIR1 leu2::LEU2+TIR1 SPC42-GFP::HphNTI hsl1-AID::TRP*	This study
DK 3327	a	*bar1Δ his3::His3MX6+TIR1 leu2::LEU2+TIR1 SPC42-GFP::HphNTI gin4-AID::KanMX6 hsl1-AID::TRP1*	This study
DK 3330	a	*bar1Δ his3::His3MX6+TIR1 leu2::LEU2+TIR1 SPC42-GFP::HphNTI gin4-AID::KanMX6 hsl1-AID::TRP1 swe1Δ::URA3*	This study
DK 3350	a	*bar1Δ GIN4-GFP:: His3MX6 SPC42-yomRuby2::KanMX*	This study
DK 3790	a	*bar1Δ gin4-ΔKA1-GFP::His3MX6 SPC42-yomRuby2::KanMX*	This study
DK 3351	a	*bar1Δ gin4-ΔKA1-LactC2-GFP:: His3MX6 SPC42-yomRuby2::KanMX*	This study
DK 3823	a	*bar1Δ gin4-ΔKA1-LactC2^{AAA}-GFP::His3MX6 SPC42-yomRuby2::KanMX*	This study
DK 888	a	*bar1Δ gin4Δ::LEU2*	(Mortensen *et al.*, 2002)
HT159	a	*bar1Δ hsl1Δ::His3MX6*	This study
DK3784	a	*bar1Δ gin4Δ::LEU2 hsl1Δ::His3MX6*	This study
DK2158	a	*bar1Δ gin4Δ::LEU2 hsl1Δ::HphNTI swe1Δ::URA3*	This study
DK 373	a	*bar1Δ GIN4-3xHA::TRP1*	This study
DK 2822	a	*bar1Δ gin4-ΔKA1-3xHA::His3MX6*	This study
DK 3286	a	*bar1Δ gin4-ΔKA1-LactC2-3xHA:: His3MX6*	This study
DK 3295	a	*bar1Δ gin4-ΔKA1-LactC2^{AAA}-3xHA::His3MX6*	This study

DK3621	a	*bar1Δ GIN4-3xHA::TRP1 hsl1Δ::HphNTI*	This study
DK3624	a	*bar1Δ gin4-ΔKA1-3xHA::His3MX6 hsl1Δ::HphNTI*	This study
DK3627	a	*bar1Δ gin4-ΔKA1-LactC2-3xHA:: His3MX6 hsl1Δ::HphNTI*	This study
DK3630	a	*bar1Δ gin4-ΔKA1-LactC2^{AAA}-3xHA::His3MX6 hsl1Δ::HphNTI*	This study

Table 2: Primers used in this study

Primer Name	Primer sequence (5' to 3')
Gin4-39	TGTGCAAAAAATTAGGGAAAAAAATGCTGGCTCGCAGGCATGCACTGAACCCCTAGGCCT
Gin4-40	ACAGCCCAGCAGCTCCACT
Gin4-41	GCACAACCGTATCACCCTGCGAGTGGAGCTGCTGGGCTGTCGGATCCCCGGGTTAATTAA
Gin4-38	AACGAAGGAGACAAAACATGATTGCATTACATTAGCACTAGAATTCGAGCTCGTTTAAAC

Table 3: Plamids used in this study

Plasmid Name	**Details**	Source
pKT1995	pRS306-GFP-LactC2^{AAA}-URA3	(Takeda *et al.*, 2014)
pKT2100	pRS306-GFP-LactC2-URA3	(Takeda *et al.*, 2014)
pAID1	AID-tagging genes at the C-terminus; Kanamycin resistance	(Nishimura *et al.*, 2009)
pTIR2	Plasmid containing the osTIR1 under the GPD1 promoter. After PmeI digestion, recombines at the *HIS3* locus	(Nishimura *et al.*, 2009)
pTIR4	Plasmid containing the osTIR1 under the GPD1 promoter. After PmeI digestion, recombines at the *LEU2* locus	(Nishimura *et al.*, 2009)
pFA6a-yomRuby2::KanMx	Yeast-optimized (yo) mRuby2	(Lee *et al.*, 2013)

Figure 1

A.

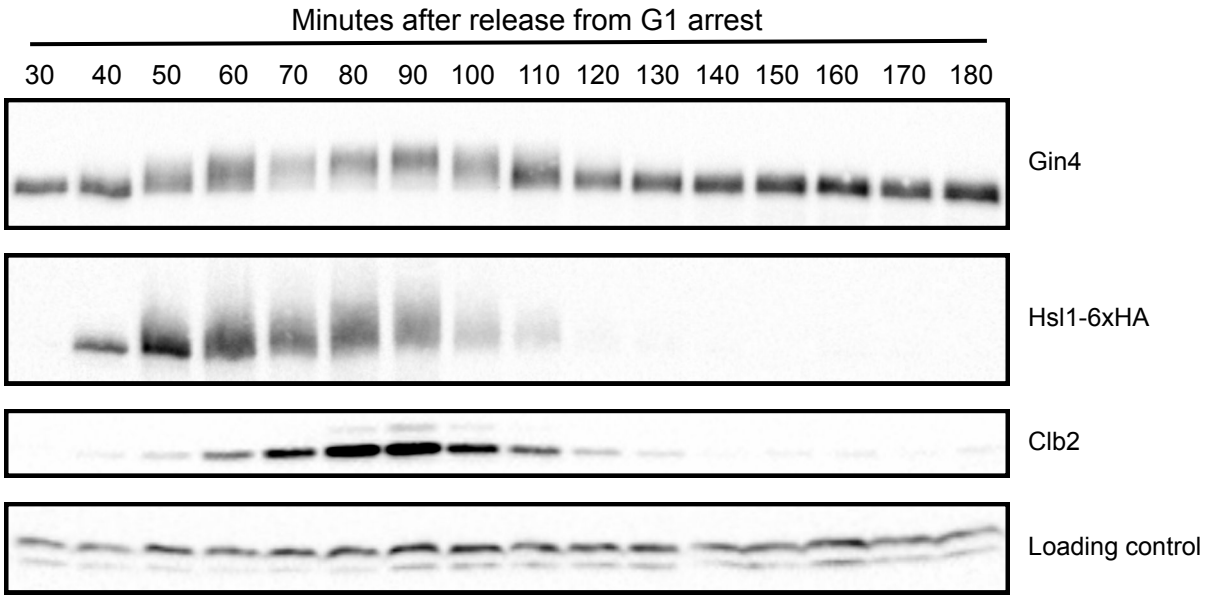
Minutes after release from G1 arrest
30 40 50 60 70 80 90 100 110 120 130 140 150 160 170 180
Gin4
Hsl1-6xHA
Clb2
Loading control

B.

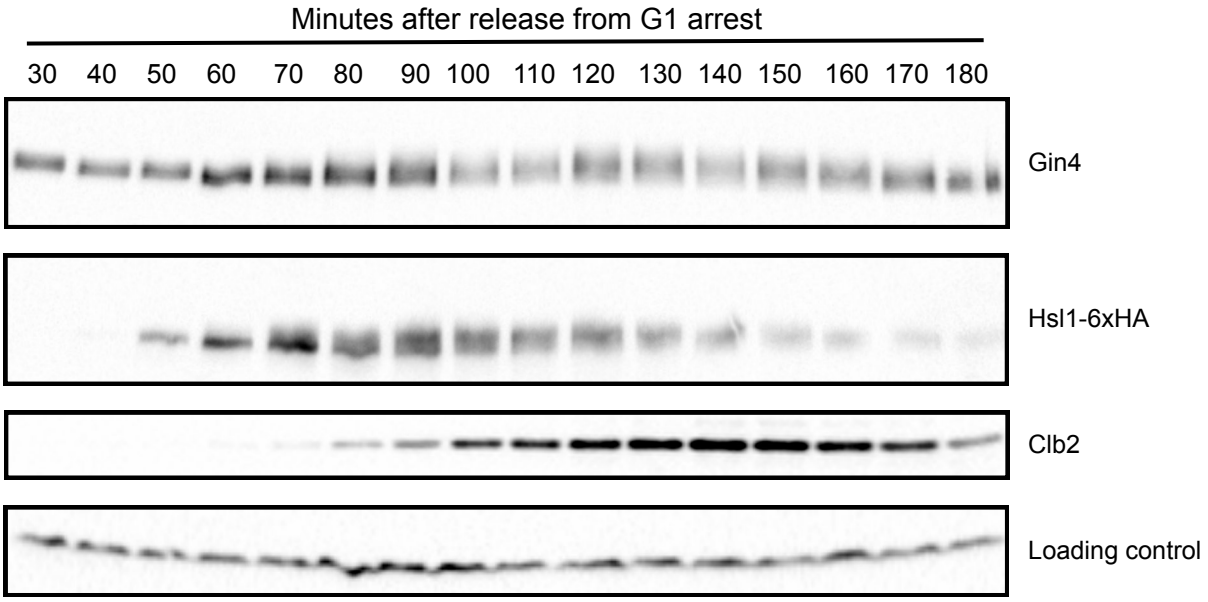
Minutes after release from G1 arrest
30 40 50 60 70 80 90 100 110 120 130 140 150 160 170 180
Gin4
Hsl1-6xHA
Clb2
Loading control

C.

Rich
Poor
Gin4
Loading control

Figure 2

A.

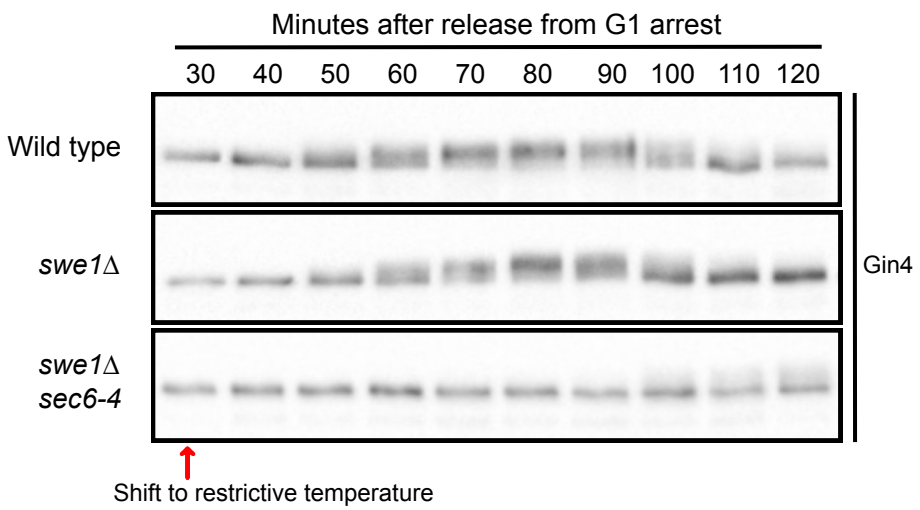
Minutes after release from G1 arrest
30 40 50 60 70 80 90 100 110 120
Wild type
swe1Δ
swe1Δ
sec6-4
Gin4
Shift to restrictive temperature

B.

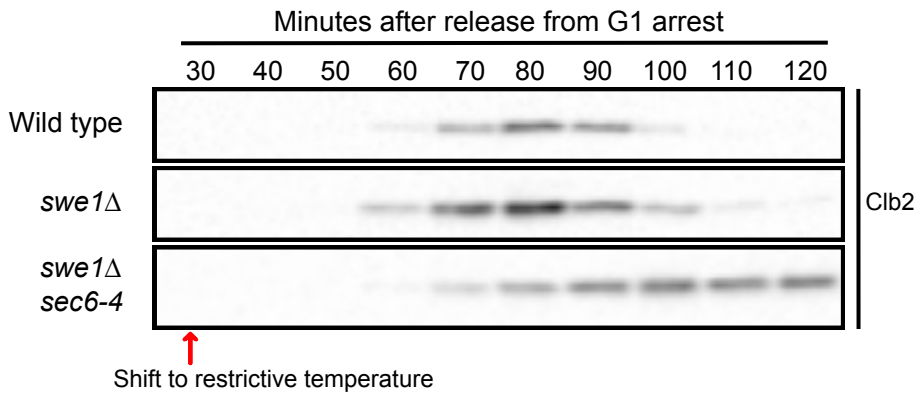
Minutes after release from G1 arrest
30 40 50 60 70 80 90 100 110 120
Wild type
swe1Δ
swe1Δ
sec6-4
Clb2
Shift to restrictive temperature

C.

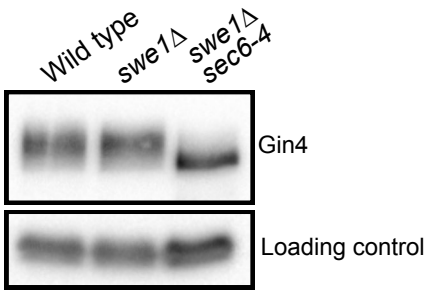
Wild type
swe1Δ
swe1Δ
sec6-4
Gin4
Loading control

Figure 3

A.

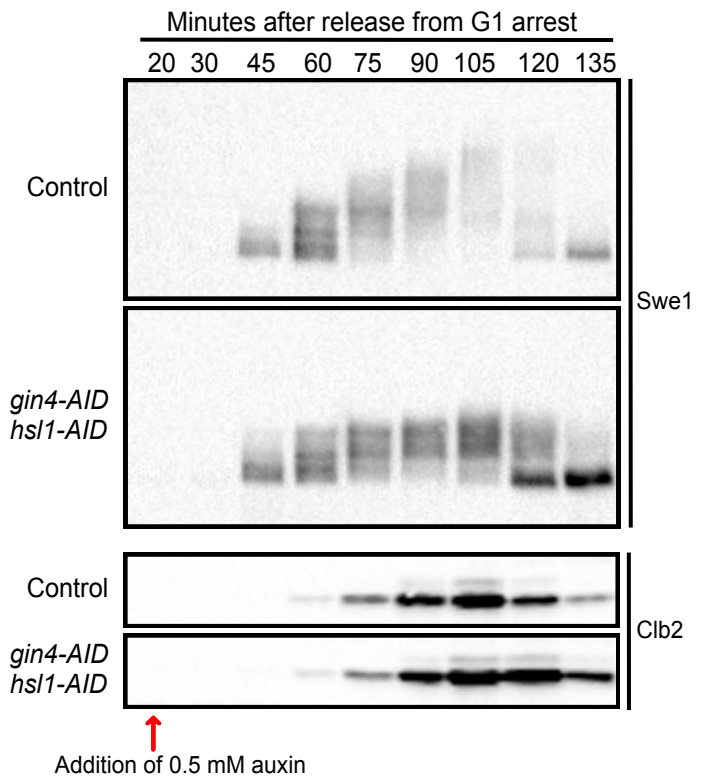
Minutes after release from G1 arrest
20 30 45 60 75 90 105 120 135
Control
gin4-AID
hsl1-AID
Swe1
Control
gin4-AID
hsl1-AID
Clb2
Addition of 0.5 mM auxin

B.

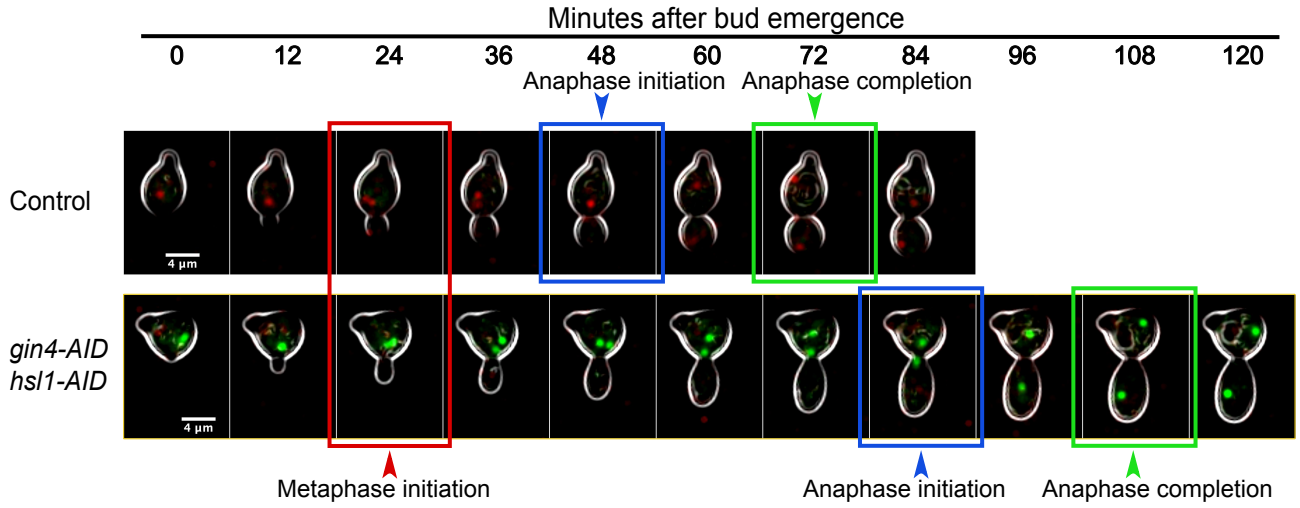
Minutes after bud emergence
0 12 24 36 48 60 72 84 96 108 120
Anaphase initiation
Anaphase completion
Control
gin4-AID
hsl1-AID
4 µm
4 µm
Metaphase initiation
Anaphase initiation
Anaphase completion

Figure 4

A.

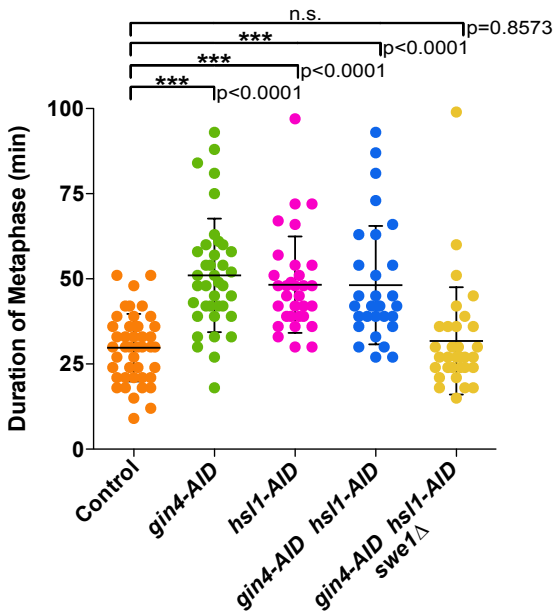

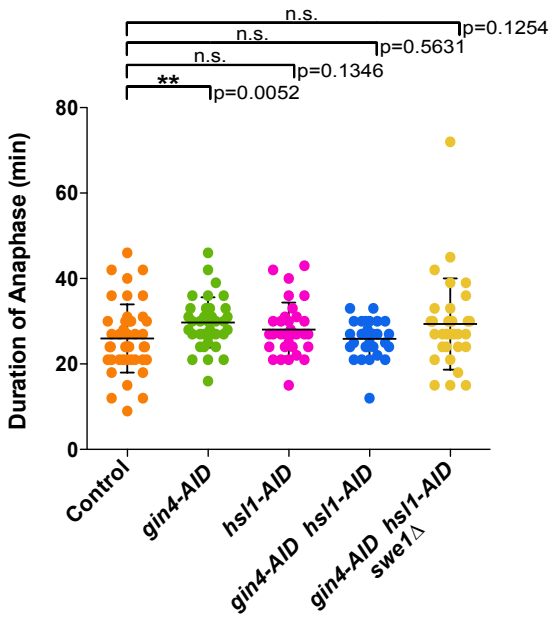

B.

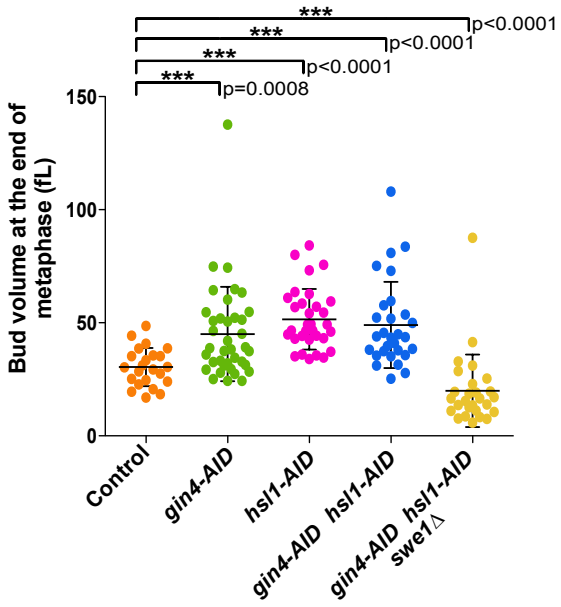

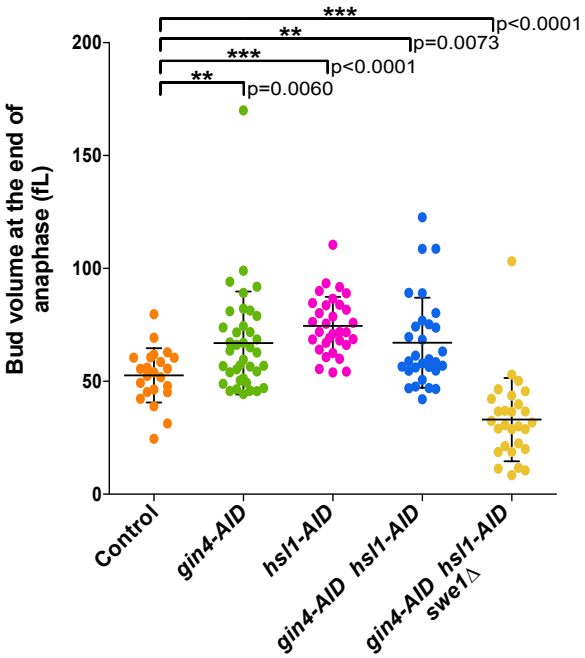

C.

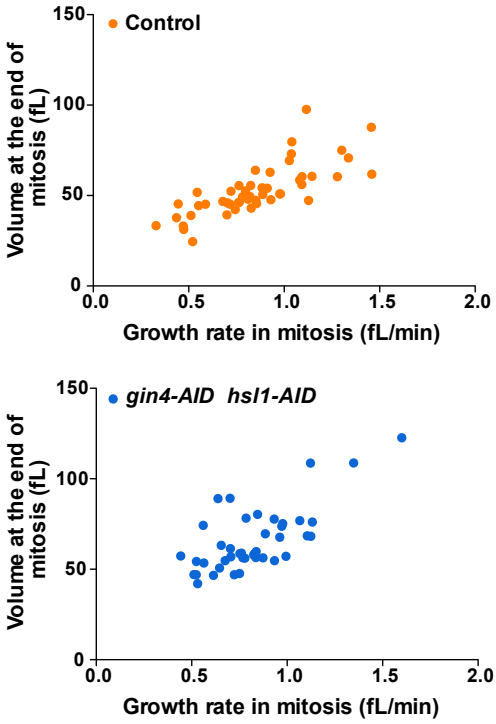

D.

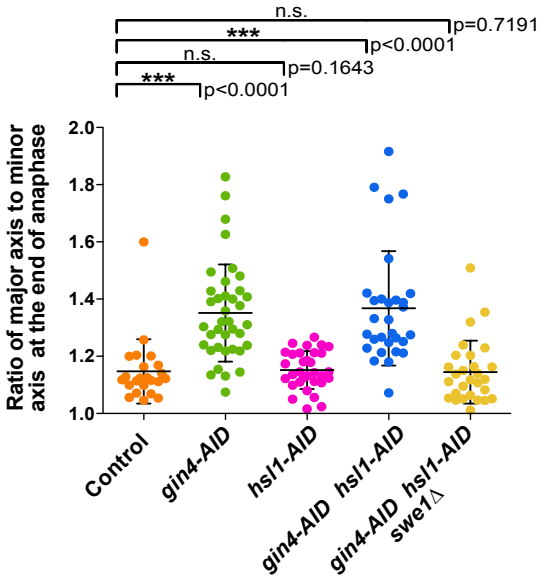

Figure 5

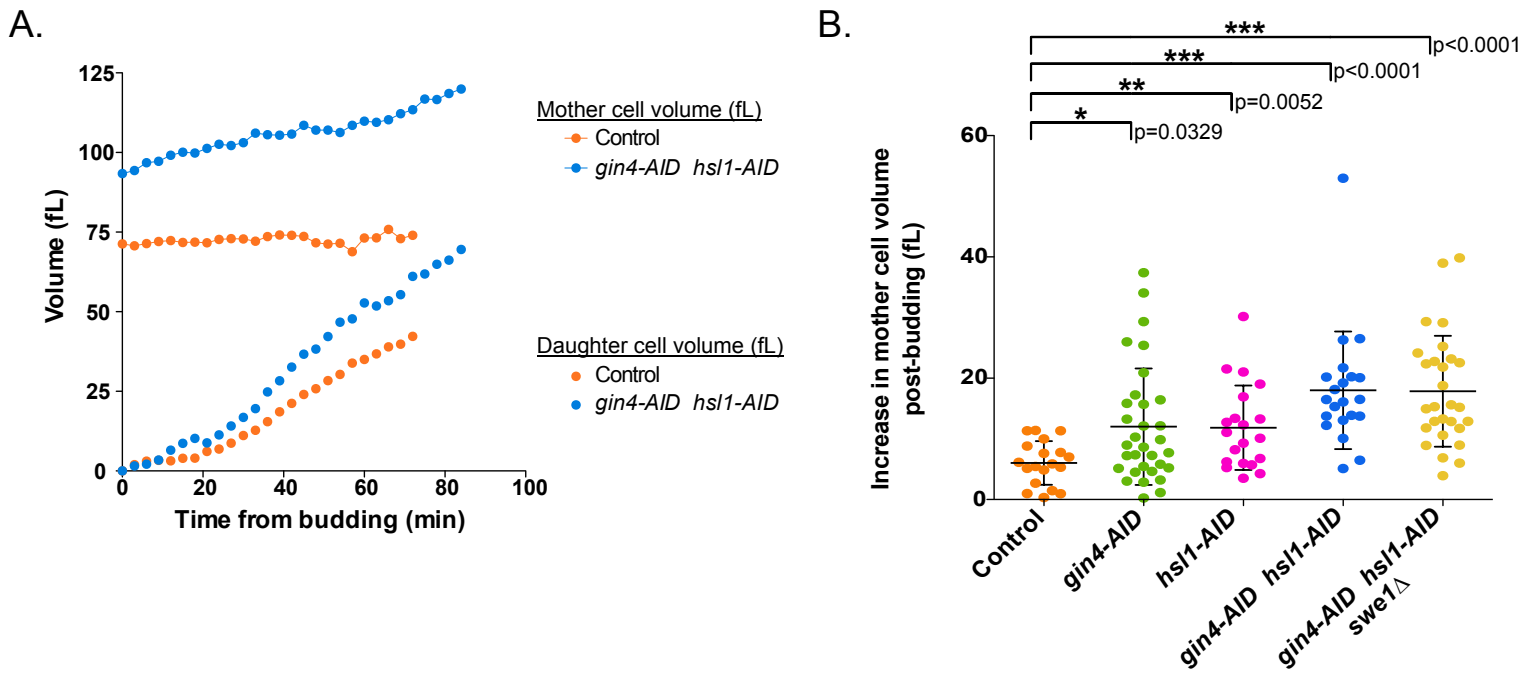
A.
125
100
75
50
25
0
Volume (fL)
0
20
40
60
80
100
Time from budding (min)
Mother cell volume (fL)
Control
gin4-AID hsl1-AID
Daughter cell volume (fL)
Control
gin4-AID hsl1-AID
B.
***
p<0.0001
***
p<0.0001
**
p=0.0052
*
p=0.0329
60
40
20
0
Increase in mother cell volume post-budding (fL)
Control
gin4-AID
hsl1-AID
gin4-AID hsl1-AID
gin4-AID hsl1-AID swe1Δ

Figure 6

A.

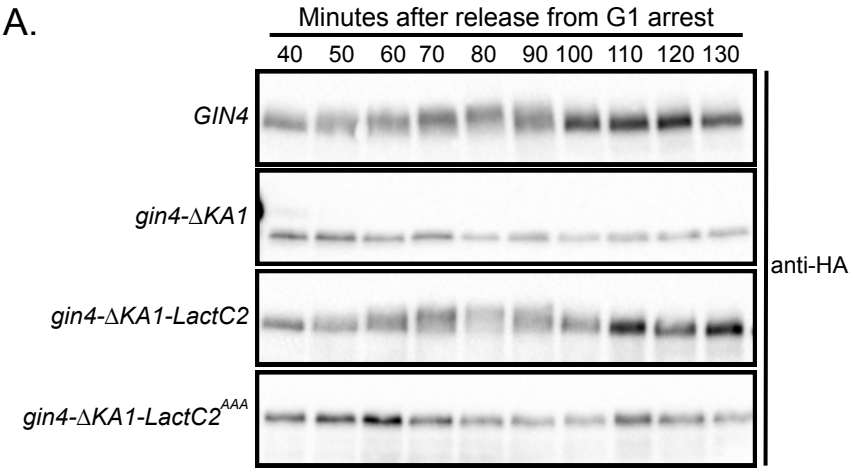

B.

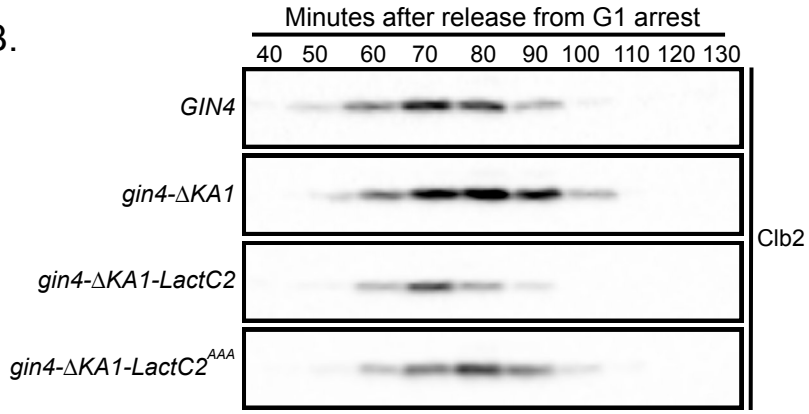

C.

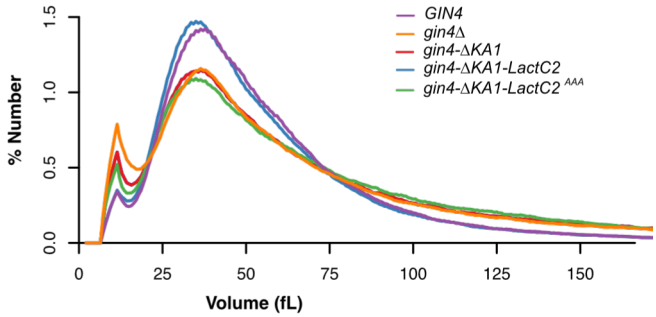

D.

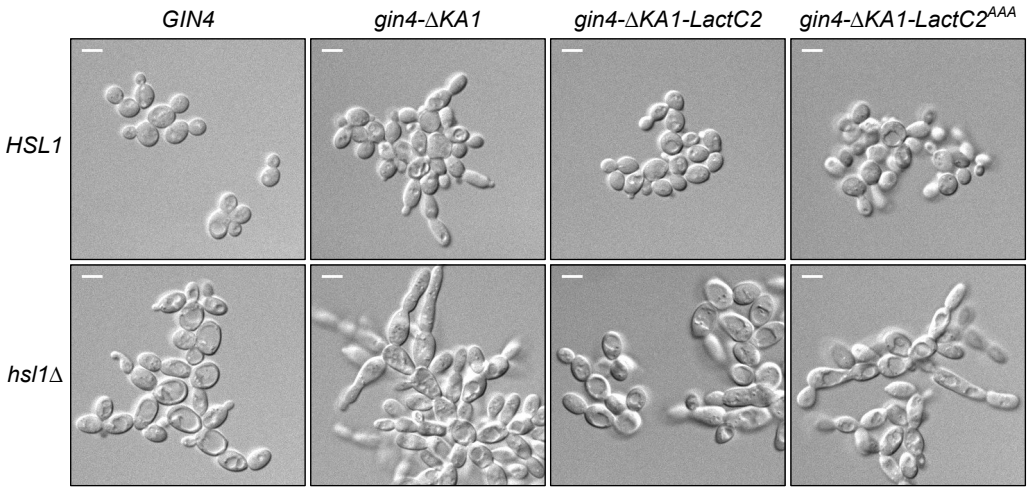

E.

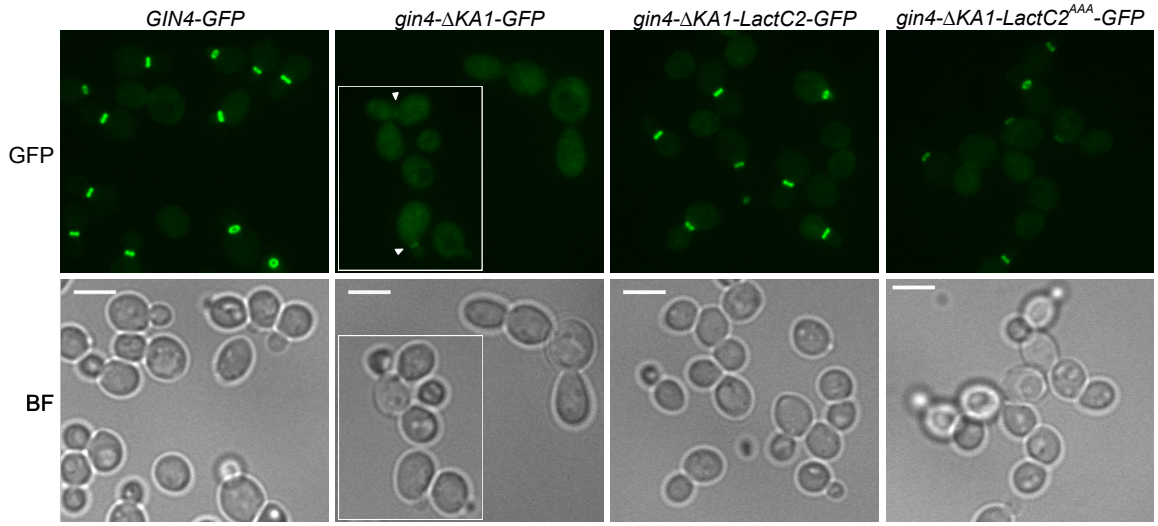

Figure S1

A.

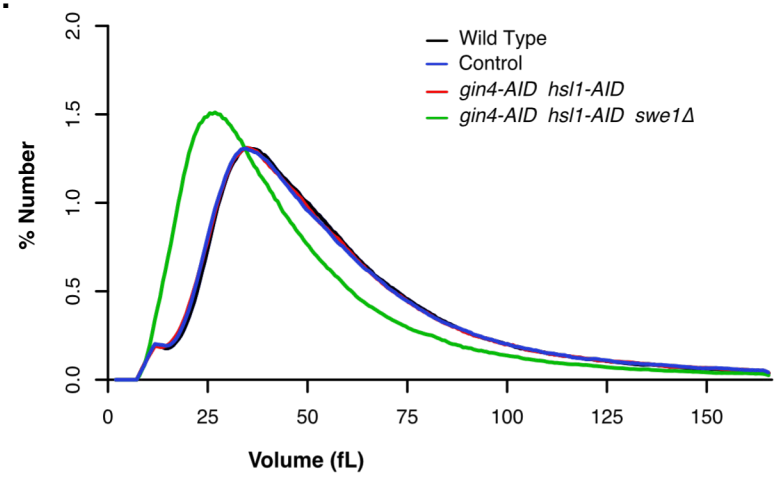

D.

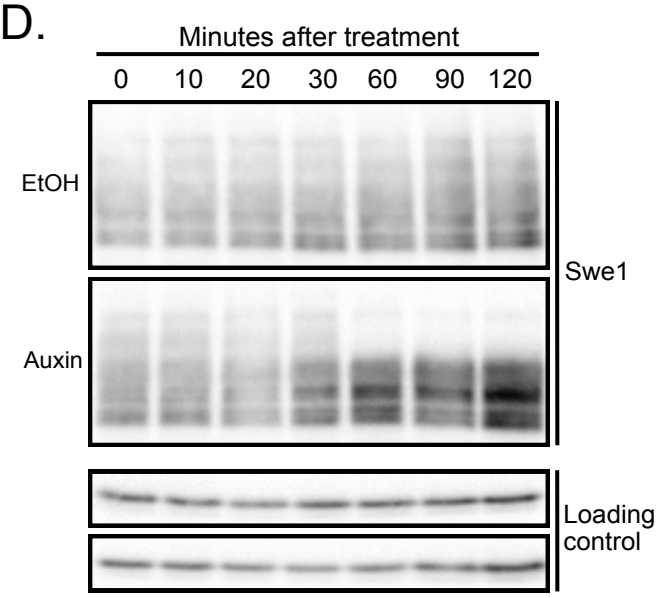

B.

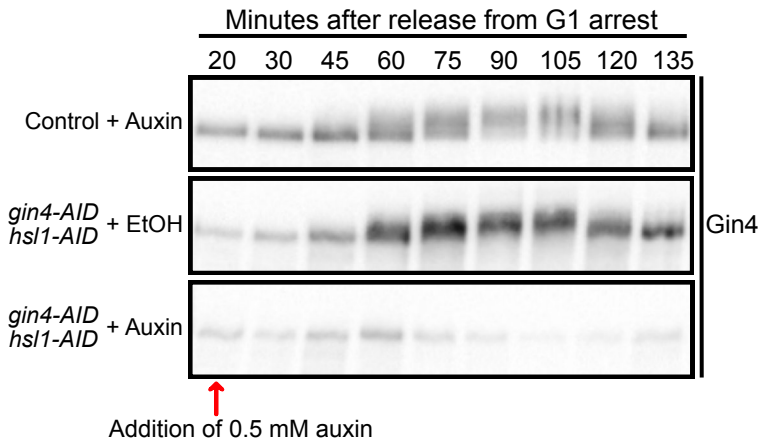

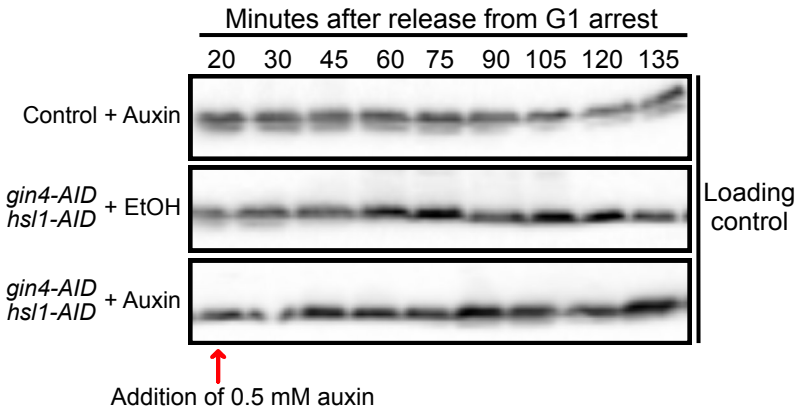

C.

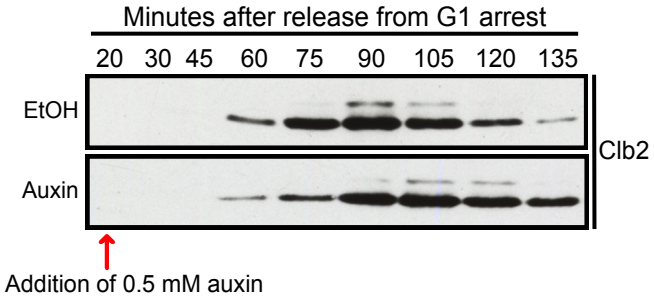

Figure S2

A.

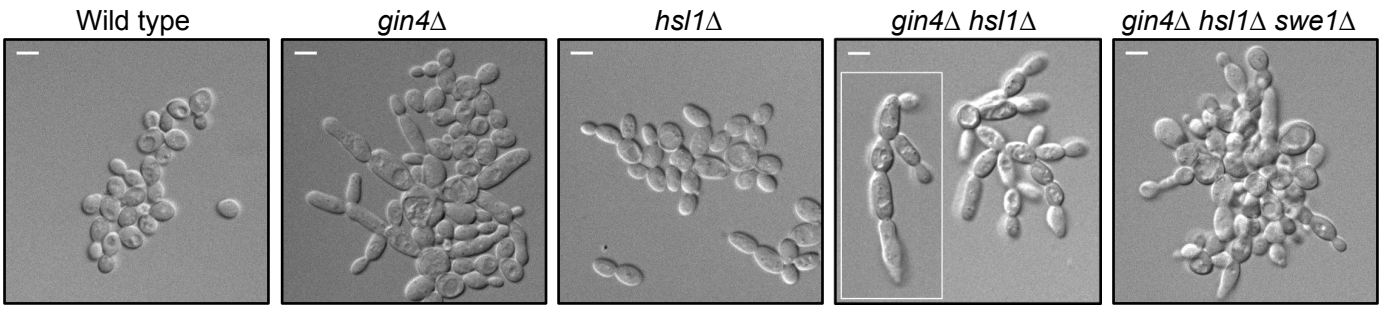
Wild type
gin4Δ
hsl1Δ
gin4Δ hsl1Δ
gin4Δ hsl1Δ swe1Δ

B.

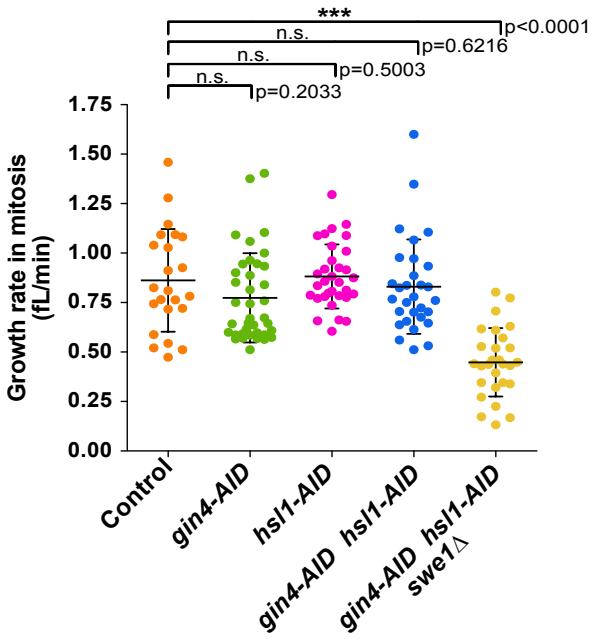
***
p<0.0001
n.s.
p=0.6216
n.s.
p=0.5003
n.s.
p=0.2033
Growth rate in mitosis (fL/min)
1.75
1.50
1.25
1.00
0.75
0.50
0.25
0.00
Control
gin4-AID
hsl1-AID
gin4-AID hsl1-AID
gin4-AID hsl1-AID swe1Δ

Figure S3

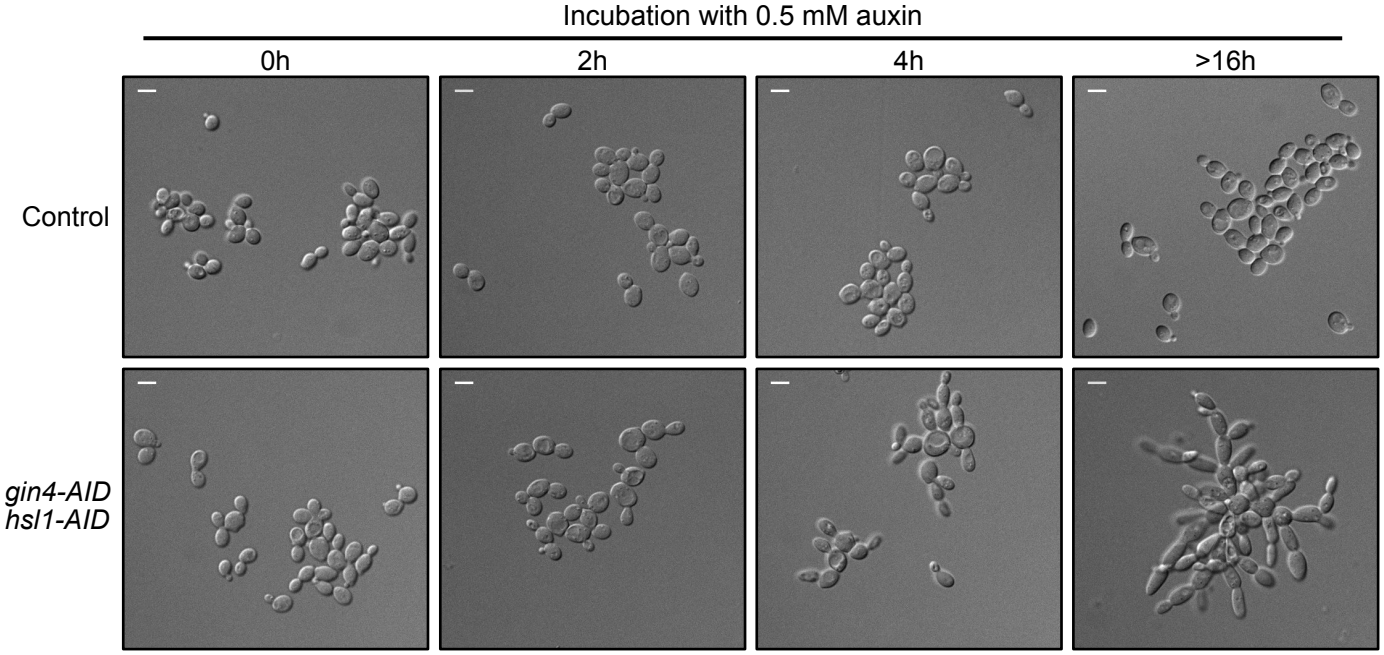
Incubation with 0.5 mM auxin
0h
2h
4h
>16h
Control
gin4-AID
hsl1-AID

Figure S4

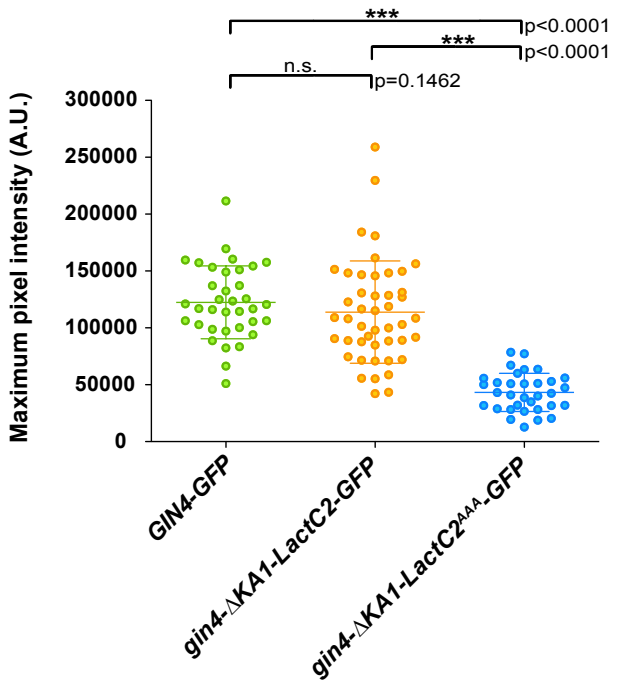
***
p<0.0001
***
p<0.0001
n.s.
p=0.1462
Maximum pixel intensity (A.U.)
300000
250000
200000
150000
100000
50000
0
GIN4-GFP
gin4-ΔKA1-LactC2-GFP
gin4-ΔKA1-LactC2AAA-GFP